Design and Numerical Analysis of Photonic Crystal Fiber Based Refractive Index Sensor

by

Tahia Tahsin - 160021051

Aadreeta Hossain - 160021053

Zareen Mustafa - 160021124

A Thesis Submitted to the Academic Faculty in Partial Fulfillment of the Requirements for the Degree of

BACHELOR OF SCIENCE IN ELECTRICAL AND ELECTRONIC ENGINEERING

Department of Electrical and Electronic Engineering

Islamic University of Technology (IUT)
Gazipur, Bangladesh
February 2021

Design and Numerical Analysis of Photonic Crystal Fiber Based Refractive Index Sensor

Approved by:

Prof. Dr. Mohammad Rakibul Islam

Supervisor and Professor
Department of Electrical and Electronic Engineering
Islamic University of Technology (IUT)
Boardbazar, Gazipur-1704.

Date: ……

TABLE OF CONTENTS

Abstract…… iii

Acknowledgement…… iv

List of Figures…… v

List of Tables…… vii

List of Abbreviations…… viii

List of Symbols…… ix

Chapter 1: Overview

1.1 Background…… 1

1.2 Problem Statement…… 2

1.3 Research Objective…… 3

1.4 Motivation…… 4

1.5 Thesis Framework…… 5

Chapter 2: Technical Background of Photonic Crystal Fiber

2.1 Overview…… 6

2.2 Evolution of Photonic Crystal Fiber…… 6

2.3 Classification of PCF…… 7

Chapter 3: Surface plasmon resonance and SPR Based Optical Fiber Sensor

3.1 Introduction…… 8

3.2 History…… 8

3.3 Surface Plasmon Wave…… 10

3.4 Surface Plasmon Resonance…… 10

3.5 Surface Plasmon Polariton…… 11

3.6 Evanescent field…………….…………………...….….……………….... 11

3.7 Surface plasmon excitation by light………………….………………. 12

  3.7.1 Prism Configuration…………………………….……….. 12

  3.7.2 Excitation of SPR in an optical fiber…………………….. 13

3.8 Reported designs……………………………………………………... 15

Chapter 4: Design and Numerical Analysis of A Gold Coated Photonic Crystal Fiber-Based Refractive Index Sensor

4.1 Introduction…………………………………………………………… 16

4.2 Structural Design and Theoretical Modeling………………………………. 19

4.3 Design Factors Controlling Sensing Performance of a SPR sensor……….. 22

4.4 Simulation Results……………………………………………………. 24

4.5 Fabrication Tolerance………………………………………………… 33

4.6 Discussion……………………………………………………………. 38

Chapter 5: Modeling and Numerical Analysis of PCF Biosensor Using Single Hexagonal Lattice Structure

5.1 Introduction……………………………………...…………………… 40

5.2 Proposed structure and Theoretical Analysis….…………………………… 41

5.3 Numerical Analysis and Discussion……………………………………….. 45

5.4 Discussion…………………………………………………………….. 48

Chapter 6: Concluding remarks and future studies

6.1 Conclusion……………………………………………………………. 49

6.2 Socio-Economic Influence…………………………………………… 49

6.3 Future studies………………………………………………………… 50

6.4 References…………………………………………………………….. 51

ABSTRACT

Over the span of past decade, photonic crystal fiber (PCF) sensors utilizing surface plasmon resonance (SPR) phenomenon have shown marvelous headway. Numerous scientists have proposed a more extensive scope of SPR-based sensors at this point. However, a considerable amount of these proposed sensors either show low affectability or it is exceptionally hard to manufacture the sensors for ongoing applications. We have developed a PCF SPR sensor that has circular-shaped air holes which is easy to fabricate as well as shows high sensitivity in the visible and near-infrared spectroscopy. We have used a layer of gold covering the cladding layer of the PCF structure to generate surface plasmon excitation. An external layer is applied to minimize emission of light from the fiber core. The guiding properties and analytical evaluation are carried out using the COMSOL Multiphysics on the basis of finite element method. In x-polarization mode, the suggested structure gives maximal value of amplitude sensitivity and wavelength sensitivity (WS) of 1757.3RIU^{-1} (Refractive Index Unit) and 32,000 nm/RIU respectively. In addition to that, the proposed design exhibits high sensor resolution of 1.428×10^{-6} and figure of merit of 587.2 indicating a high-performance sensor and demonstrates birefringence of 0.004 RIU. Moreover, the proposed PCF-SPR sensor is composed of only six symmetrical circular air holes, which makes it fabrication friendly. For our next design, we have focused on reducing confinement loss and simultaneously increase wavelength sensitivity. Here we have used a single layer of hexagonal shaped lattice with circular air holes. The proposed design gives maximal AS of 1072.5 RIU^{-1}, peak WS of 41,000 nm/RIU, and sensor resolution of 2.4×10^{-6} considering the x-polarization mode. The high performance of the proposed sensor and high fabrication probability makes the sensor a strong contender to be used in biomedical and biochemical applications.

ACKNOWLEDGEMENT

All praise to the almighty Allah (SWT). By the grace of Him, we were able to conclude our assigned thesis with noteworthy results.

Throughout the writing of this thesis we have sustained an inordinate dispense of support and assistance. First, we would like to thank our supervisor, Professor Dr. Mohammad Rakibul Islam, whose prowess was indispensable in contriving the research questions and methodology. His perceptive feedback motivated us to polish up our intelligence and elevated our work. We would also like to thank all our tutors from the department of Electrical and Electronic Engineering, for their enlightened guidance throughout our studies. They imparted us with the tools that we needed to go for the right direction and successfully complete our thesis. They provided us with constructive criticisms and precious propositions wherever required. In addition, we would like to thank our parents for their wise pointers and sympathetic ear. They were always there for us. They provided happy distractions to rest our minds outside of our research.

LIST OF FIGURES

Figure 2.1: (a) Photonic crystal fiber for sensing application. (b) Mono-radial annular core photonic crystal fiber (c) photonic crystal fiber…………………………………..……(7)

Figure 3.1: Generation of surface plasmon wave…………………………......…………(10)

Figure 3.2: Surface plasmon resonance phenomenon…..………………………..………(11)

Figure 3.3: (a) Otto configuration (b) Kretschmann configuration……………………..…(13)

Figure 3.4 (a)-(d) : SPR fiber sensors……………….……………………….…………..(14)

Figure 4.1: (a) Cross-sectional aspect (2D) where d_1=1.96µm, d_2=0.6µm, t_g=35nm, t_a=0.82µm and t_p=1.2µm and (b) air-hole distribution of the suggested PCF SPR based biosensor...…(19)

Figure 4.2: (a) Core-guided form (b) surface plasmon polariton form in x-polarized mode; (c) Scattered relation of primary core form and SPP form……………………..…………….(21)

Figure 4.3: Variation in CL and AS due to gold thickness for analyte refractive index η_a = 1.38 and 1.39…………………………………………………………............................(25)

Figure 4.4: Variation in CL and AS due to change in analyte thickness (sensing length) at analyte refractive index η_a = 1.38 and 1.39……...…………………………………......(26)

Figure 4.5: Variation in confinement loss and amplitude sensitivity due to change in PML depth at analyte refractive index η_a = 1.38 and 1.39…………….........………..…..……(27)

Figure 4.6: Variation in confinement loss and amplitude sensitivity due to change in diameter of center/large air holes at analyte refractive index η_a = 1.38 and 1.39……………….……(28)

Figure 4.7: Variation in confinement loss and amplitude sensitivity due to change in diameter of extra/small air holes at analyte refractive index η_a = 1.38 and 1.39……..………...…(29)

Figure 4.8: Variation in confinement loss and sensitivity due to change in analyte refractive index (1.33-1.39)…………………………..……………………..(30)

Figure 4.9: (a) Change in sensor length with increment of analyte RI; (b) Regression line for resonance wavelength variation with analyte Refractive Index..…………………...………(32)

Figure 4.10: Loss spectrums for variation in (a) gold layer thickness, (b) analyte thickness, (c) PML thickness, (d) diameter of cladding air hole (e) diameter of small air hole in the x-polarization mode…………………........……………………………………….………(35)

Figure 4.11: Step by step fabrication of the proposed fiber in stack and draw method (capillary stacking process)………………………………….....…………………….…...….(36)

Figure 4.12: Step by step fabrication of the sensor (Drawing process)……..……………......(37)

Figure 5.1: Cross-sectional 2D view of the proposed fiber………………………………..(41)

Figure 5.2: (a) Core-guided mode and (b) SPP mode for x-polarization (c) Dispersion between fundamental mode and SPP mode……………………………………………………......(42)

Figure 5.3: CL versus AS due to change in (a,b) analyte RI from 1.33 to 1.40, (c,d) gold thickness (e,f) diameter of small air holes, and (g,h) diameter of air holes in the cladding region…………………………………………………………………………..…..(46)

Figure 5.4: Visual illustration of working mechanism of PCF sensor…………………….(47)

LIST OF TABLES

Table 3.1 Difference in sensor performance based on various structural lattice 15

Table 4.1 AS variation with the alteration of gold layer thickness 24

Table 4.2 AS variation with the alternation of sensing medium layer 25

Table 4.3 AS variation with the alteration of PML layer thickness 26

Table 4.4 AS variation with the alteration of diameter of center/large air holes 28

Table 4.5 AS variation with the alteration of diameter of extra/small two air holes 29

Table 4.6 Performance Analysis by altering analyte refractive index from 1.33-1.40 31

Table 4.7 Comparative analysis of the suggested sensor and prior stated sensor 38

Table 5.1 Comparing results of Proposed sensor with prior sensors 48

LIST OF ABBREVIATIONS

PCF	Photonic Crystal Fiber
SPR	Surface Plasmon Resonance
SPP	Surface Plasmon Polariton
SPW	Surface Plasmon Wave
FEM	Finite Element Method
RI	Refractive Index
AS	Amplitude Sensitivity
WS	Wavelength Sensitivity
RIU	Refractive Index Unit
CL	Confinement Loss
EMI	Effective Material Index
THz	Terahertz
CVD	Chemical Vapor Deposition
TiN	Titanium Nitride
TiO_2	Titanium Dioxide
Au	Gold

LIST OF SYMBOLS

n	Refractive index
λ	Wavelength
ε	Permittivity
μ	Permeability
ω	Angular frequency
γ_D	Damping frequency
ω_D	Plasmon frequency
$\Gamma_L/2\pi$	Spectral width
α	Modal loss
k_0	Wave number
$\alpha(\lambda, n_a)$	Confinement loss
λ_{min}	Minimum wavelength resolution
L	Sensor Length
B	Birefringence
ε_{Au}	Permittivity of gold(Au)
n_x	Effective mode index(EMI) for x-polarized mode
n_y	Effective mode index(EMI) for y-polarized mode

Chapter 1: Overview

1.1 Background

Due to the availability of digital optical instrumentation optical biosensors are broadly used to observe and examine the biomolecular interaction. In the late 80s, the very first optical biosensor had been advertised. The core objective of an optical sensor is light-based where optical strength or electromagnetic fields varies due to the presence of various specimens. Conversion of optical rays into electrical signals is possible with the help of advanced machinery that is able to convert the optical rays into electrical signals which determine the variation and response of ambient condition or to compute the strength of electromagnetic radiation called an optical sensor. For this purpose, few optical sensor approaches such as surface plasmon resonance, resonant mirrors, and evanescent wave absorption spectroscopy are accessible. However, SPR circumstances have gained much recognition due to its wide range of applications and high sensitivity.

Surface plasmon resonance-based optical sensor operates initially by generating the surface plasmon wave. This entire operation basically occurs when the frequency of the generated wave matches the incident light frequency of the polarization or transverse magnetic (TM) wave which results in the resonance of free electrons generated from the metal surface. These free electrons impart the real part of a negative permittivity necessary for plasmonic materials. The initial purpose of a waveguide is to conduct electromagnetic waves with the least possible receivable transmission loss and almost negligible scatterings at any desired wavelength. Many waveguides have been discovered over the years for efficient THz wave proliferation, low loss and dispersion such as several metallic waveguides (single metallic wire, parallel plate photonic waveguide, circular/rectangular waveguide, parallel plate waveguide, coaxial waveguide) [1], dielectric metal-coated glass tube [2], hollow-core Bragg fiber [3], dielectric polymer fiber [4] etc. Researchers also discovered sensor applications in electro-optical devices such as modulators, SPR images, biosensors, gas sensors and liquid sensors.

Surface plasmon resonance (SPR) based optical biomolecular sensors provide one of the most up-to-date label-free sensing technologies [5]. Their potential to inspect and observe the interaction between a static molecule on the sensor surface and an interacting fellow molecule in an aqueous solution resulted in SPR sensors being quite important in the optical sensor for biomolecular interaction inspection and biomolecular experiment [6]. So far, among the multiple applications that SPR sensors possess perception of biochemical and organic substances in the medical sector, environmental or military sector can be highlighted. Instrument platforms have been more and more developed since the introduction of SPR sensors [7]. Diversity of availability of monetary SPR sensors includes high-resolution sensors easing one of the challenging research into biomolecular interaction with the more untangled and economically effective result for fast detection [8].

Different types of optical fiber-based SPR sensors have been announced due to their detailed range of applications as well as improved sensing property and precision. During the last decade, a SPR sensor-based microstructured optical fiber has been revealed for the very first time. Photonic crystal fiber (PCF) based SPR sensing technique is considered as a possibly easier way to sensor minuteness and thus, it has been proven as a good replacement of prism. By tackling its advantages such as small size, simpler light generation, single-core mode propagation, and control over evanescent field, PCF turns out to be an encouraging possibility for the SPR sensor sector.

1.2 Problem Statement

To date, various SPR sensing elements are reported. Most of the structure of the reported sensors are quite sophisticated to be invented because of selective coating of metal layers and liquid infiltration within the air-hole surface to manage the light propagation in a specific direction these sensors introduced oval-shaped air-holes, and conjointly many tiny air-holes within the specific position that makes the sensors structure advanced in terms of fabrication.

Being an effective field of analysis, many styles for SPR primarily based optical device had been implemented by the researchers and noticeable development had been discovered. Although the internal sensing technique provides higher sensitivity than an external one, it's expensive and incorporates an advanced structure. Thus, so far, the constraints that were ascertained for the SPR based mostly optical sensors are fabrication problem, weak evanescent field, complicated design for high sensitivity and high loss.

Thus, most of the structure of the proposed sensors were tough to be fabricated thanks to a selective coating of metal layers and liquid infiltration within the air-hole surface and the performance of those sensors square measure discovered by following the within sensing. Several PCF SPR sensors were conjointly discovered where the metallic and sensing layer are placed outside the fiber structure to modify the sensor configuration. However, to manage the light propagation in a specific direction to reinforce the temporary field, these sensors introduced noncircular air-holes and conjointly many small air-holes square measure by selection placed within the specific position that makes the sensors structure complex in terms of fabrication operation. On the contrary, achieving high sensitivity with having a relatively low loss remains a challenge for these sensors.

1.3 Research Objective

The focus of our thesis was to investigate contemporary SPR-based designs and mould an appraisal focusing on those researches to acknowledge SPR phenomenon and its concomitant term properly and to augment our own designs depending upon that in order to dispense a genuine and reliable solution for the following-mentioned problems. In explicit, the objectives of the analysis are as follows:

✓ To attain high sensitivity with a very low confinement loss

✓ Proposing a structure that follows an external sensing approach and may guide robust evanescent field

✓ To investigate the potential of the projected sensors supported wavelength and amplitude interrogation technique.

✓ Fabrication friendly.

1.4 Motivation

This research is entirely subsidized by simulation works. All orchestrated sensors are audited using the COMSOL software and functioning are perfected with wavelength interrogation and amplitude interrogation strategies. The precision of the simulation procedures is demonstrated with the divulged literature before investigating the planned sensors. Proposed PCF SPR sensors are progressed by scrutinizing the selected metal coating, liquid infiltration and internal sensing issues.

Surface plasmon resonance allows the sensitive detection of biomolecular interactions directly while not having to label probe molecules with fluorescent markers or the utilization of color-changing substrates that allows tons of applications for it. It is often accustomed to perform DNA and ribonucleic acid assays by noticing interactions of the complementary base pairings in real-time. It will take a look at the presence of viruses like an infectious disease in blood samples by sensing reactions with virus-specific antigens. It performs biology on one aspect and physics on the opposite. On the biology aspect, biomolecules square measure mobilized on the surface of the gold film act as molecular probes and on the physics aspect, infrared emission creates a resonance with surface plasmons within the film making a minimum and mirrored optical strength at a selected angle.

SPR technology is often democratized, creating out there to everybody within the instrument that is quick, correct and straightforward to use. It is often used to examine antibody-antigen, bacteria, virus, DNA, RNA, mRNA, hemoglobin, hormone, macromolecule etc. It also can be used in close to future in physics, physical science and software packages. So, one will specialize in its applications in biological sector, physics, biology and education. Having a huge field to research and conduct analysis with it in physics or biology or chemistry, SPR technology is one in all the foremost promising analysis space at present.

1.5 Thesis Framework

This dissertation report is collocated into six chapters. A synopsis of the chapters are included in this section.

Chapter 2 provides the fundamental introduction of photonic crystal fiber (PCF) and its evolution in optical fiber technology. Different kinds of PCF that are presently being employed is mentioned with mentioning the variations of PCF primarily based on fiber from the standard one. Finally, the method, algorithms that are used to simulate the result and the code that has been used in our research work are discussed in short.

Chapter 3 presents detailed data of what is SPR, its background history. However, SPR forms through surface plasmon wave (SPW), resonance and generates surface plasmon polariton with the assistance of an evanescent field. This section is over with describing the various structures and their impact on the sensing element.

Chapter 4 and chapter 5 is the core part of our thesis which projected a SPR sensor primarily based fiber style which may fulfill our analysis objective. Two design structures are given and comparative analysis among them is provided. All the results that are obtained from the simulation of the accomplished design structure are plotted and mentioned and compared with the antecedently according styles.

Chapter 6 presents the conclusion, socio-economic impact and alternative projected future works.

Chapter 2: Technical Background of Photonic Crystal Fiber

2.1 Overview

In this chapter, we conferred a short discussion of Photonic Crystal Fiber (PCF), classification of PCF, the distinction between PCF-based fiber and traditional fiber, light-guiding mechanism of PCF. We additionally mentioned some structural properties

2.2 Evolution of Photonic Crystal Fiber

Photonic Crystal fibers (PCF) measures fibers with a periodic transversal microstructure. In 1978, the idea of photonic crystal fiber was given for the very first time by Yeh et al. They planned to clad a fiber core with Braxton Bragg grating that is comparable to 1D photonic crystal. PCFs are in sensible existence since 1996 as low-loss waveguides. It took four years of technological development for the initial demonstration and since then the techniques of fabrications changing into a lot of sophisticated producing the microstructure in air-glass PCF to accuracies of 10 nm on the dimensions of 1 μm is currently attainable.

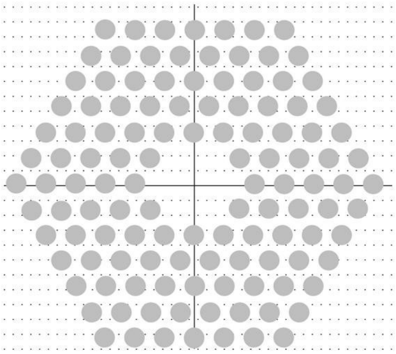

(a)

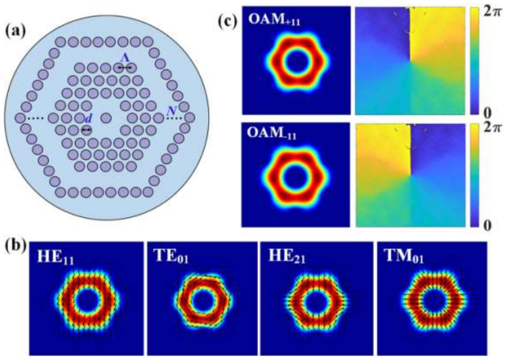

(b)

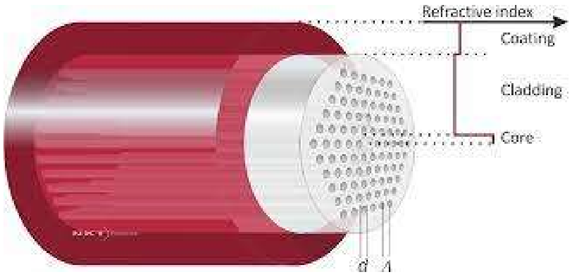

(c)

Figure 2.1: (a) Photonic crystal fiber for sensing application. (b) Mono-radial annular core photonic crystal fiber (c) photonic crystal fiber

PCF encompasses a nice variation of prospects by introducing new features like low-loss guidance during a hollow core.

2.3 Classification of PCF

PCFs are often classified into many sorts. The classification depends on the structures, fiber parameters and specific guiding properties [12]. PCFs are typically diverged into two main categories: Index-Guiding Fibers (IG-PCF) and Photonic Bandgap Fibers (PBG-PCF). Index Guiding PCFs or IG-PCF consists of many sorts like, extremely nonlinear fibers or HNL fibers which include tiny core dimensions to confirm tight mode confinement. High Numerical aperture fibers or HNA fibers include a microstructure protective covering and a hoop of air holes surround the cladding and bigger mode space fibers or LMA fibers which includes a larger dimension of the core and little index of refraction to confirm a bigger effective area. Hole-aided PCFs (HAPCFs) is another style of IG-PCF once IG-PCFs have a doped core which has high index doped silica and a porous protective covering. Photonic bandgap Fibers (PBG-PCFs) square measure of various categories like, Air-Guiding fiber (AG fiber) or Hollow Core (HC fiber) and LIC fibers or general fibers.

Chapter 3: Surface Plasmon Resonance and SPR Based Optical Fiber Sensor

3.1 Introduction

Surface Plasmon resonance (SPR) is an optical-based, label-free detection technique for periodic observation of binding interactions between more than one molecules. Being a physical method SPR can occur once light hits a metal film beneath the total internal reflection conditions when the resonant oscillation of conductivity electrons at the interface between negative and positive permittivity material stirred up by incident light. Binding interactions between a molecule on the device surface and its binding partners in the resolution are monitored in a period by SPR. Once the molecules bind, the index of refraction near to the surface alters inflicting a shift within the angle of minimum mirrored intensity. SPR-based biosensors will be powerful tools for the portraiture of molecular interactions. The amalgamation of three individual parts, the detector, the device surface and also the sampled delivery system is crucial to the complition of the experiment.

3.2 History

In the late sixties, the physical phenomenon of surface plasmons through attenuated total reflection (ATR) was shown by Kretschmann and Otto [9-13]. Optical excitation of surface plasma waves has two major approaches: attenuated total reflection in prism coupler-based structures and optical phenomenon at optical phenomenon gratings. Significantly, as a result of its comparative coherence, this technique has been widely applied for the characterization of thin films [13-14] and organic chemistry sensing [15-17]. In the 1980s, SPR and correlated techniques were appealed to the interrogation of thin films and additionally for biological and chemical interactions [13]. These techniques permit the user to review the interaction between immobilized receptors and analytes in resolution, in real-time and while not labeling the analyte. By observant binding rates and binding levels, there are other ways to provide data on the specificity, dynamics and affinity of the interaction, or the concentration of the analyte. In 1980, Pharmacia got interested in SPR and began to work with the probabilities of the method. In 1983, SPR sensors were introduced for the primary time by Liedberg et al that was based on prism coupling [7]. Later in 1984, Pharmacia supported the corporate Pharmacia Biosensor AB to come up with and market a purposeful SPR-machine. The event of acceptable sensor surfaces by Pharmacia Biosensor [18-19] and therefore the manufacturing of the atomic number 14 microfluidic cartridge brought AN easy-to-use SPR-machine nearer to changing into a reality [20]. Over the years, different makers developed alternative SPR systems. Within a brief amount, several researches from Pharmacia Biosensor introduced the latest colloidal gel of dextran [21] the interconnection between the SPR signal and therefore the RIA assay [22] and gave a specification of the BIACORE machine [23]. BIACORE instruments used a wedge-shaped laser beam and a diode array for detection, which ends in no moving elements within the detection unit. The development of various, unique, additional sensitive and specialised machines gave U.S.A. the BIACORE X, BIACORE 2000, 3000 and letter of the alphabet for internal control. Alternative developments concerned the way the liquid was handled.

SPR detector provides greater sensitivity. Thus, even a really little change of associate analyte's RI will be found through peak wavelength shift. Higher sensitivity results in higher accuracy of detection of the associated unfamiliar analyte. Plasmonic (sensing) material plays an important role in SPR detector performance. It is used as the sensing material for the surface plasmon resonance phenomenon. It guides the incident light-weight from the cladding part to the metal-dielectric surface to produce the surface plasmon wave which ends up in the surface plasmon polariton. As SPR is employed for mainly sensing within the molecular level, this material must be exceptionally stable in nature and additionally fabrication of it within the fiber got to be compatible.

Generally silver, copper and gold is used as active plasmonic materials [24]. The use of silver material ends up in a pointy resonance peak that will increase accuracy of the sensing. But it is chemically unstable and extremely prone to getting oxidized that scales back the sensing performance [25]. A skinny coating of graphene layer is often used as a stronger answer however it's terribly advanced to fabricate and the price is relatively higher. Gold is with chemicals stable as a result of it does not oxidize easily [26]. It additionally shows a slender resonance peak than different out there materials. So far several noticeable works are introduced to enhance the performance of the SPR detector.

3.3 Surface Plasmon Wave

SPR sensors area unit comprehended of a glass substrate and skinny gold coating. Light travels inside the substrate and is mirrored off the gold coating. At particular angles of incidence, a part of the light energy couples through the gold coating creates resonant oscillation of physical phenomenon electron and resulted in an exceedingly surface plasmon wave at the interface of sample and gold surface (Jiri Homola, 2006).

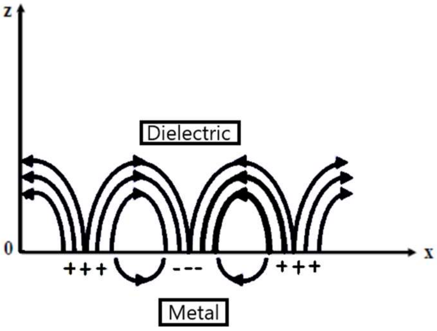

Figure 3.1: Generation of surface plasmon wave

The angle of incident light needed to sustain the surface plasmon wave is extremely sensitive to changes in the index of refraction at the surface and conjointly with the thickness of the layer of the sample and also the gold. These are the changes that the area unit required to monitor the association and dissociation of biomolecules. Thus, the surface plasmon wave is that the main basis of surface plasmon resonance.

3.4 Surface Plasmon Resonance

Surface plasmon resonance (SPR) refers to the excitation of surface plasmons (SPs) of electromagnetic waves coupled on the surface within a metal and a nonconductor medium propagated over the interface of the metal and nonconductor material. The surface plasmon can be exhilarated by the evanescent wave. Once this happens, the intensity of the reflected light-weight decreases extensively. Excited surface plasmon decays embody energy conversion to photons [27].

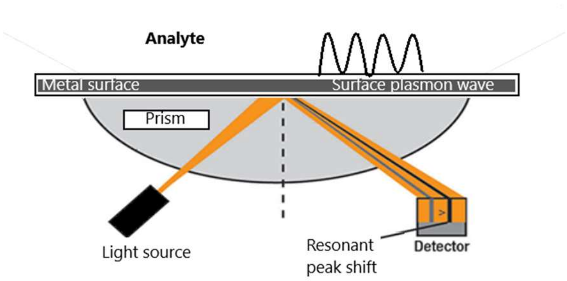

Figure 3.2 : Surface plasmon resonance phenomenon

The fundamental operation mechanism of PCF-based SPR sensors depends on the mutual interaction between evanescent field and surface electrons. The evanescent field guides the binding of the molecules that create the SPW. In short, SPW interacts with the sensing layer because of this phenomenon.

3.5 Surface Plasmon Polariton

The charge motion in a very surface Plasmon invariably creates magnetism fields inside and outside the metal. The whole excitation, together with each the charge motion and associated electromagnetic field is Surface plasmon polariton. Surface plasmon polaritons (SPPs) are infrared or visible frequency magnetism waves, which travel along with a metal-dielectric or metal-air interface. The term Surface Plasmon Polariton explains that the wave involves each charge motion within the metal (Surface Plasmon) and electromagnetic waves within the air or dielectric (Polariton). SPP can propagate on the interface till its energy is lost either to absorption within the metal or scattering into different directions [28].

3.6 Evanescent Field

For reflection of light at particular angles close to the angle of incidence, a big section of the facility extends into the facing or medium surrounding the core. This development, called the evanescent wave extending solely to a brief distance from the interface with power dropping exponentially with distance. Fiber optics are typically aforesaid to use total internal reflection for guiding the optical energy down the fiber. However a little of the internally reflected wave extends a little distance on the far side of the core boundary into the optical facing. This is the evanescent wave property, which can be exploited by removing the fiber facing to permit the evanescent wave to increase on the far side of the core boundary into substances close to the fiber core.

3.7 Surface Plasmon Excitation by Light

In order to electrify SPR by irradiation with light, a phase-matching condition ought to be persuaded stating that the excitation of SPR is feasible provided that the propagation constant of the optical vector complements the propagation constant of the SPs [29]. As per the plasmon dispersion relation [30] for any wavelength, SPs have an extended wave vector than light waves of identical frequency propagating at the surface. This condition makes it not possible to excite SPs directly by shining incident light onto a sleek metal surface. Though, in the last few years there has been a lot of limelight to excite SPR on the surface of optical fibers and sub-wavelength holes [31]. Prism coupling is one in all the primary tested SPR configurations and is mentioned in the resulting section.

3.7.1 Prism Configuration

Many years back, Otto introduced a prism coupling technique wherever the prism and metal were placed in an exceedingly gap and also the gap was full of the sample liquid that ought to be smaller than the prism. Otto configuration follows the attenuated total reflection (ATR) technique. To utilize this prism-coupling, prism and metal layer ought to be placed with a finite gap that could be a disadvantage of Otto-configuration.

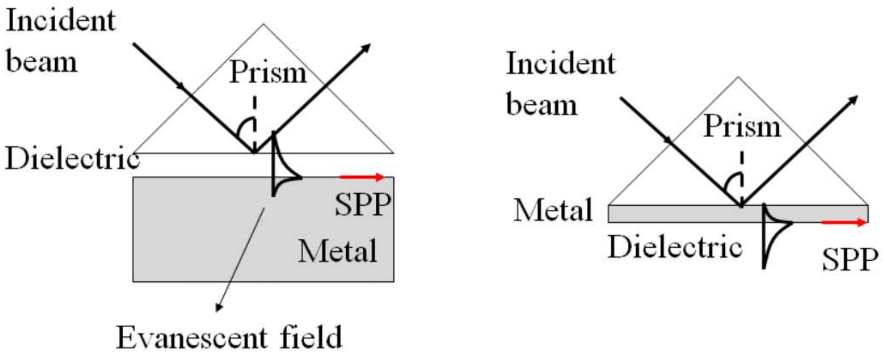

Figure 3.4: (a) Otto configuration (b) Kretschmann configuration

By resolution of this downside, a changed configuration is introduced that is thought of as Kretschmann configuration. In this methodology, the prism and metal layer was connected along the prism and metal layer without any gap. For any selected angle once the wave vector of evanescent wave and also the surface plasmon wave matched then the resonance occurred, at this resonance condition a dip mirrored intensity additionally appeared. However, the prism-based mostly SPR sensing element within the well-known Kretschmann set-up is large and not appropriate for remote sensing. Hence, PCF has been tried as a decent replacement of prism.

3.7.2 Excitation of SPR in Optical Fibers

Considering sensors presently based on Kretschmann configuration may be comparatively tiny, there has been an effort to excite SPR in glass fiber to supply a lot of compact and reliable sensors with remote sensing capabilities. Excitation of SPR in optical fibers is analogous to the excitation of SPR within the prism configuration. Light propagation within the fiber core and protection in the form of modes expertise total internal reflection at the cladding-core and cladding-exterior medium interfaces. Totally different modes hit the cladding-core and cladding-exterior medium interfaces at totally different angles.

Recently, exceptional inprovement has been created to SPR, localized SPR and photonic crystal fiber technologies, new styles of glass fiber SPR-based sensors been getting much attention within the research community. As a result, it is unimaginable to go through all possible factors in these areas. The details and a few wonderful reviews on a number of the studies may be found within the references [32-35]. Some of the overall SPR fiber sensors area units shown in Figures 3.7(a) - (d).

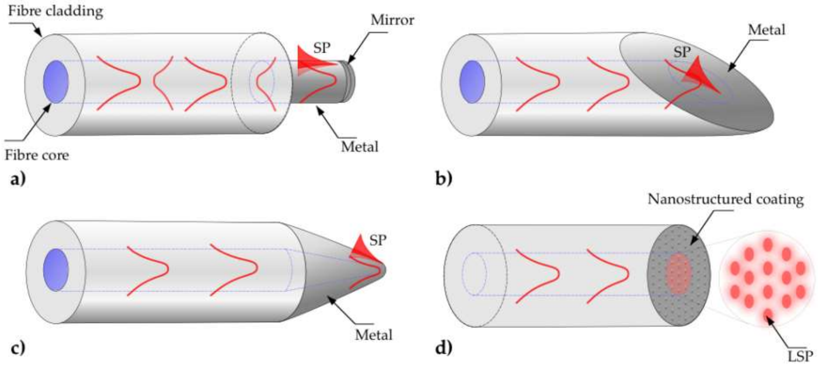
Fibre cladding
Mirror
SP
Fibre core
Metal
a)
Metal
SP
b)
Nanostructured coating
SP
Metal
c)
d)
LSP

Fig 3.5 (a)-(d) : SPR fiber sensors

It is the evanescent wave that produces the first condition for the physical phenomenon electron the metal-dielectric interface to oscillate at the resonant frequency. A weak evanescent field means a higher core power fraction, which ends in an exceedingly light-weight unable to an incident on sensors supporting the quality single mode fiber without deforming or modifying.

3.8 Reported designs

Over the course of the time of ceaseless innovative work, SPR sensors have formed into the present structure. From Table 3.1 we can see some previously published work and their results.

Table 3.1

Difference in sensor performance based on various structural lattice

Reference	Lattice Type	Sensing Approach	Analyte Refractive Index Range	Maximum Amplitude Sensitivity (RIU^{-1})	Maximum Wavelength Sensitivity (nm/RIU)	Maximum Sensor Resolution (RIU)
35	Hexagonal	External	1.36-1.40	19000	910	5.26×10^{-6}
36	Hexagonal	External	1.33-1.37	4000	320	3.125×10^{-5}
37	Hexagonal	External	1.33-1.37	1000	118	8.5×10^{-5}
38	D-Shaped	External	1.43-1.46	9000	-	1.30×10^{-5}
39	D-Shaped	External	1.18-1.36	20000	1054	5×10^{-6}
40	D-Shaped	External	1.345-1.410	12450	-	-
41	Circular	External	1.33-.139	8000	198	1.25×10^{-5}
42	Circular	External	1.37-1.41	12000	2044	8.33×10^{-6}
43	Circular	External	1.33-1.43	62000	1415	1.61×10^{-6}
44	Hybrid	External	1.35-1.38	4500	347	2.22×10^{-5}
45	Trapezoidal	External	1.40-1.44	17000		
46	Spiral	External	1.33-1.38	4600	420.4	2.69×10^{-5}
47	Random	External	1.33-1.345	5000	500	2×10^{-5}

Chapter 4: Design and Numerical Analysis of A Gold-coated photonic crystal fiber-based refractive index sensor

4.1 Introduction

Biosensors are analytical devices that consolidate biological components with chemical detectors. Since last decades, biosensors found on surface plasmon resonance (SPR) are comprehensively developed and implemented compared to other sensing technologies, for instance, PCF sensors [48-53], fiber Bragg grating (FBG) sensors, photoluminescence, micro-ring resonator, resonant mirror [54] [31]. On a metal-dielectric interface under a total internal reflection state, a TM (transverse magnetic) or also termed as p-polarized incident light generates a longitudinal oscillation termed as surface plasmons. When the frequencies of both the incident light and the conduction electrons of a metal get aligned, we get an optical event termed as Surface plasmon resonance (SPR). SPR sensor provides a diverse array of applications in biological science, chemical science, gaseous phase, environment, and beyond as it offers instant detection capacity, more accuracy, real-time monitoring, and label-free detection [55]. Moreover, SPR sensors are economically efficient and easy to evaluate. SPR sensors are exceedingly sensitive to the slightest change of the value of analyte refractive index (RI); therefore, it can detect an unknown substance by investigating the resonance peak shift in response.

Conventional SPR sensors are based on prism coupling since prism can actuate surface plasmons. Kretschmann configuration sensing technique is predicated on the angular interrogation method, where impinging light is concentrated on metal through a lens [56]. Even though prism-based sensors are cost-effective, they involve bulky and complicated machinery equipment. Hence, they are not compatible with remote sensing applications and curved surfaces [57]. A particular form of optical fiber is used instead of a prism known as photonic crystal fiber (PCF), in which the cladding region contains periodic air-holes. The evanescent field traverses these air holes and strikes the metal surface. Consequently, on the metal-dielectric interface surface plasmon oscillations are generated. A significant advantage of this sensor is adaptability because the core-guided leaky-mode propagation along with the evanescent field can be restrained [58][59], and it is much smaller in size compared to prism-based sensors.

In SPR sensors, plasmonic materials are used as they exhibit negative real permittivity that eventually facilitates resonance. In general, gold, silver, aluminum, copper are extensively utilized as plasmonic materials. Silver is an extremely conductive material, has a low material loss and the resonance peak is more precise. But silver is unstable as it gets oxidized readily [60]; thus, it hampers the performance of the sensor [61]. Copper is the second most conductive material. Although copper is cheaper than other materials, it has an oxidation problem that makes it impractical [62]. Sometimes a thin bimetallic layer is added atop the silver layer to avert oxidation. On the contrary, gold shows more chemical stability than silver in any environment. Likewise, gold has a broader resonance peak, higher accuracy, and sensitivity [63]. Veerpal Kaur et al. stated an external sensing SPR PCF sensor with TiN coating, for a RI range from 1.385-1.40 with AS and WS of 70 RIU^{-1} and 10,000 nm/RIU respectively [64]. Also Yashar Esfahani Monfared described a SPR PCF sensor where the same plasmonic material gave an amplitude sensitivity of 206.25 RIU^{-1} and a wavelength sensitivity of 16275 nm/RIU [65]. With the advance of research on PCF-SPR sensors, numerous designs have been developed with high wavelength sensitivity, high sensor resolution, and ease of fabrication. Till now various types of PCFs have been explored by researchers including nano-wire based [66], internally glazed [67], D fashioned [68], and externally glazed [69]. Internal sensing approach has been more common in case of research which has yielded a wide range of new PCF-SPR sensors. An internally glazed birefringent sensor with wide range analyte Refractive Index revealing was proposed by Liu et al. which exemplified wavelength sensitivity of 6,300nm/RIU [70]. An irregular SPR sensor for analyte RI detection was proposed where the maximum WS and sensor resolution attained was 22,000nm/RIU and 4.54×10^{-6} RIU respectively [71]. A D-shaped PCF sensor exhibiting a sensitivity of 10,493nm/RIU was proposed by Guowen et al [72]. In a more recent paper Yashar et al. proposed a D-shaped SPR sensor which exhibits very high wavelength sensitivity of 11800 nm/RIU and an amplitude sensitivity of 820 RIU^{-1}[73]. Mahfuz et al. proposed a simple hexagonal lattice plasmonic biosensor with two ring air-holes with a peak value of wavelength sensitivity and peak resolution of 12,000 nm/RIU and 8.33×10^{-6} RIU respectively [74]. Another design that is dual-polarized showed maximal wavelength sensitivity of 30,000 nm/RIU [75]. Moreover an internal sensing paper was suggested by Rifat et al. [37]. But internal sensing is not suitable. So, the research branched out to external sensing producing exemplary results. A graphene-coated fiber considering external sensing giving maximum wavelength sensitivity of 5,000nm/RIU was proposed by Dash et. al [76]. A simple Au-TiO_2 based PCF-SPR sensor was proposed with wavelength sensitivity of 25,000 nm/RIU and ease of fabrication [77]. Another design comprising of a center air hole was proposed that showed wavelength sensitivity of 18,000nm/RIU [78]. By the external sensing technique with a wavelength sensitivity of 62000nm/RIU was put forward [79]. Although these sensors are proposed, none of these are yet fabricated. The first fabricated PCF SPR sensor showed a wavelength sensitivity of 2000 nm/RIU for a RI range from 1.38-1.41 [80]. In this sensor gold was implemented as the plasmonic material. Elizaveta Klantsataya et al. proposed and fabricated an exposed core microstructured optical fiber (ECF) that showed a sensitivity of 1800nm/RIU [81]. Silver was the plasmonic material in this case. Wei Chang Wong et al. fabricated a gold covered SPR sensor with a highest sensitivity of 3692nm/RIU [82]. A major section of the sensors are very difficult to fabricate and for internal sensing method, deposition of the gold layer outside the air hole is challenging. To overcome these problems, D-shaped PCFs are proposed where metal coating problem is solved. But this type of PCFs requires accurate polishing. Sensors with external sensing solve all these problems. But to acquire proper light guiding and higher sensitivity elliptical air holes need to be used. That is why in recent times researchers are trying their best to introduce external sensors having circular air holes with high sensitivity. These types of sensors are also very easy to fabricate. In this paper, a form of single square lattice PCF having circular shaped air holes and a gold layer is designed and numerically examined. By changing different geometrical parameters, maximum performance parameters are obtained.

4.2 Structural Design and Theoretical Modeling

The initial design is actually made based on the existing literature and existing designs. As our main goal is to design a SPR sensor that provides high sensitivity, the initial design should be such that it does not match with any existing design with regards to airhole placement. The initial design is not optimized and it may show better results after the optimization. That is why the whole design is then optimized varying the thickness and width of airholes, plasmonic layer etc to provide enough guiding of light to ensure better result in sensitivity.

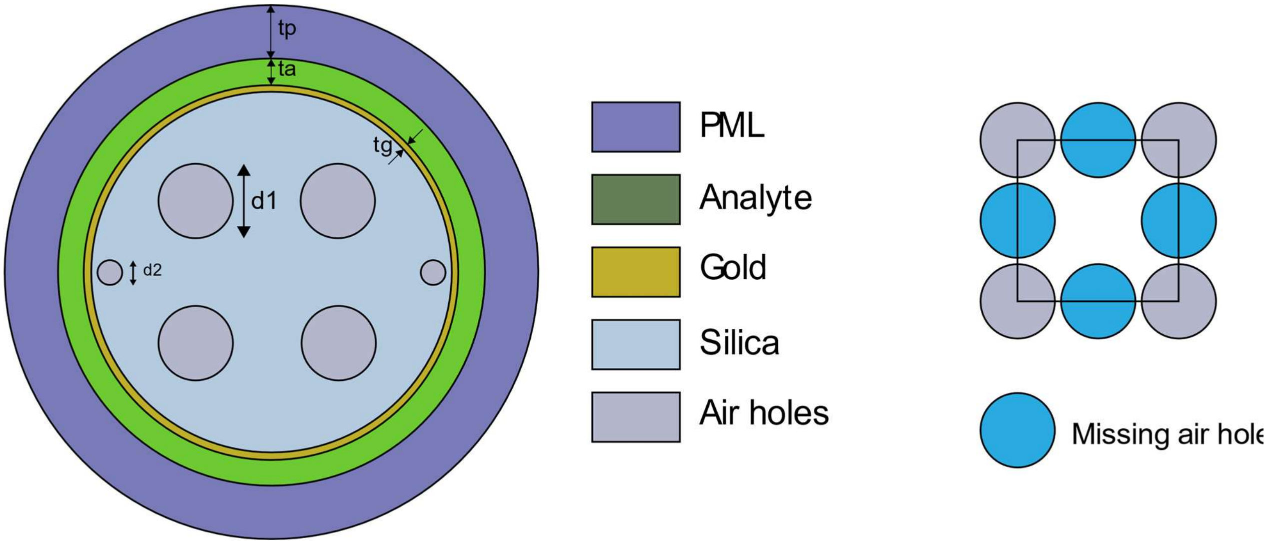

(a) (b)

Figure 4.1: (a) Cross-sectional aspect (2D) where $d_1 = 1.96\mu m$, $d_2 = 0.6\mu m$, $t_g = 35nm$, $t_a = 0.82\mu m$ and $t_p = 1.2\mu m$ and (b) air-hole distribution of the suggested PCF SPR based biosensor

Here, Fig. 4.1 demonstrates a cross-sectional aspect of the suggested square lattice SPR based sensor. Opposite air holes from both sides are eliminated to ensure a steady flow of the evanescent field. In order to secure the maximum metal excitation two additional air holes are used specifically on the x-axis. Diameter of the existing air holes from the square layer is denoted by $d_1 = 1.96\mu m$ and the diameter of the additional airholes is given by $d_2 = 0.6\mu m$. Analyte encircling a fine narrow gold layer is placed outside the core of the fiber and the width of the gold layer is indicated by $t_g = 35nm$. Analyte serves as a sensing medium, and its thickness ($t_a = 0.82\mu m$) is selected based on the convergence test.

4.3 Design Factors Controlling Sensing Performance of SPR Sensors

We have fused silica composed of a non-crystalline silica glass is used to surround the material, and its refractive index varies with the varying wavelength. It can be proved by Sellmeier equation [83]

$$n^2(\lambda) = 1 + \frac{B_1\lambda^2}{\lambda^2 - C_1} - \frac{B_2\lambda^2}{\lambda^2 - C_2} - \frac{B_3\lambda^2}{\lambda^2 - C_3} \tag{1}$$

Here, *n and* λ (µm) cites refractive index and wavelength in vacuum of fused silica (SiO_2) respectively. Sellmeier coefficients are respectively B_1 = 0.69616300, B_2 = 0.407942600, B_3 = 0.897479400, $C_1 = 4.67914826 \times 10^{-3}$ µm^2, $C_2 = 1.35120631 \times 10^{-2}$ µm^2 and C_3 = 97.9340025 µm^2. The relative permittivity of gold can be certainly figured out using the Lorenz-Drude model [84].

$$\varepsilon_{Au} = \varepsilon_{\alpha} - \frac{\omega_D^2}{\omega(\omega + j\gamma D)} - \frac{\Delta\varepsilon.\Omega_L^2}{(\omega^2 - \Omega_L^2) + \mathrm{j}\Gamma_L\omega} \tag{2}$$

In this equation, ε_{Au} is expressed as permittivity of Au, ε_{α} is expressed as permittivity at higher frequencies and the value is 5.9673. Then angular frequency is denoted by $\omega = 2\pi c/\lambda$. The damping frequency is denoted by γ_D, the plasmon frequency is denoted by ω_D and rest of the parameters of the equation are $\gamma_D/2\pi = 15.92THz$, $\omega_D/2\pi = 2113.6\ THz$, $\Omega_L = 650.07THz$ and the spectral width is denoted by $\Gamma_L/2\pi = 104.86THz$.

The PML layer with a width of 10% of the PCF structure and limiting conditions are applied to take in the transitory field dispersed out of the structure. The proposed sensor is modeled and numerically investigated by available COMSOL Multiphysics 5.4 software that implements finite element method (FEM). The computational domain subdivided the structure into 23120 triangle elements, 1752 edge elements with lowest quality of 0.5402, average quality of 0.8517, element area ratio of 0.01317, and mesh area of 156.3 µm^2.

PCF based sensors are developed based on coupling SPP (surface plasmon resonance) mode and primary core mode. Surface plasmon waves generated between metal-dielectric interfaces is the key aspect of this structure. At resonant wavelength, maximum energy transfers from the fundamental mode to the SPP mode. Evanescent field of *x*-polarized and *y*-polarized mode diversifies with the geometry of the PCF fiber [40]. In this proposed sensor, we considered x-polarization as the fundamental mode due to its peak modal loss compared to y-polarization. Moreover, the evanescent field and excitation produced by y-polarization are lower than x-polarization.

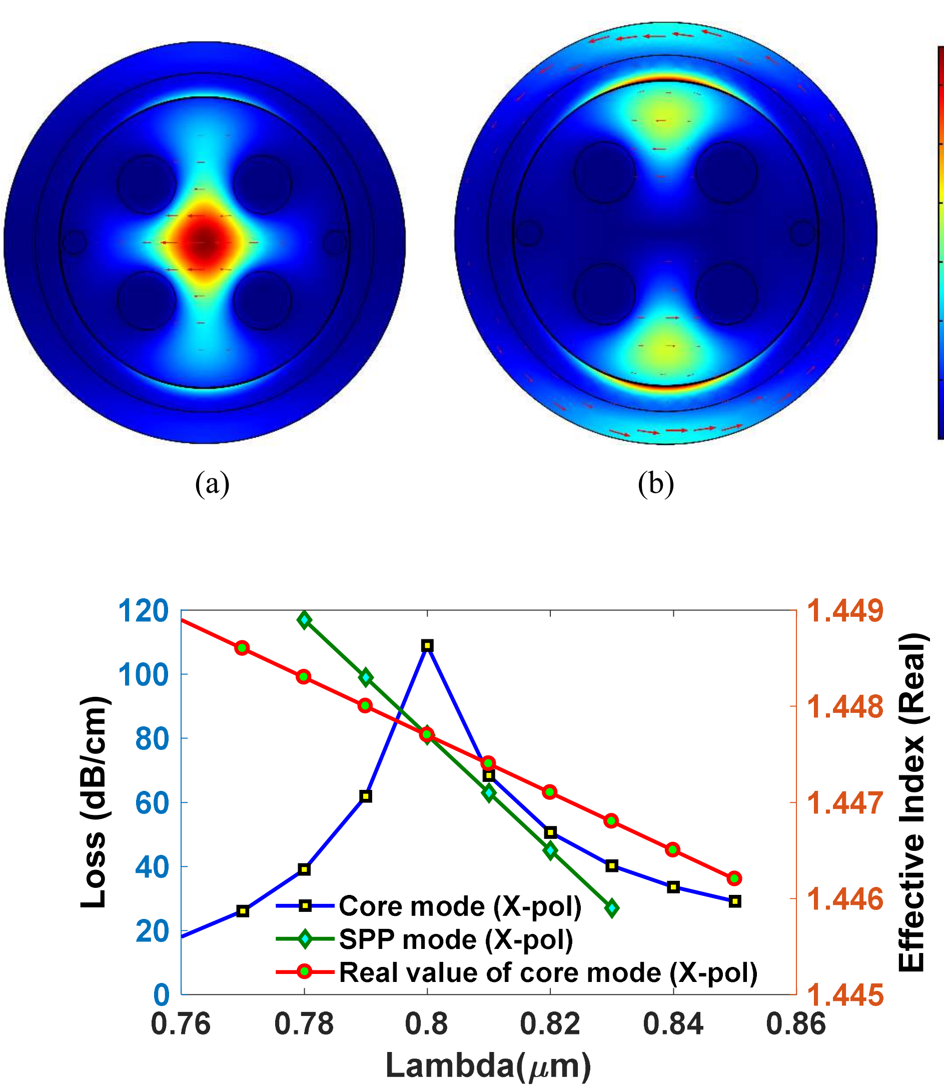

(a) (b)

(c)

Figure 4.2: (a) Core-guided form (b) surface plasmon polariton form in x-polarized mode; (c) Scattered relation of primary core form and SPP form

Fig. 4.2 (a) and Fig. 4.2 (b) demonstrates the arrangement of the core-guided form electric field and SPP form at analyte refractive index 1.39, respectively. Fig. 4.2 (c) expresses the scattered relation at Refractive index of 1.39 for x-polarization mode. Both practical refractive indices of core form and SPP form decrease when wavelength increases. At 800nm wavelength, the core-guided form and the SPP form coincide. As the crossover point stage is perfectly matched, and maximum energy transformation transpires from core form to SPP form. Thereby at that particular point, confinement loss of core mode is found to be the highest. The modal loss is determined by the following calculation [85]

$$\alpha = 40\pi.\mathrm{Im}(\mathrm{n}_{eff})/(\ln(10)\lambda) \approx 8.686 \times k_0.\mathrm{Im}[\mathrm{n}_{eff}] \times 10^4 \, dB/cm \tag{3}$$

where, $k_0 = 2\pi/\lambda$ is the wavenumber in the void.

Sensitivity can be deployed as a means of measurement of the conduct of any sensor which is PCF-based. Apart from a sensorgram curve being a suitable means for computing the susceptivity of a sensor, we propose using the amplitude and wavelength interrogation method for the detection of the sensitivity of the sensor. Nonetheless, the wavelength interrogation method is spectral-based, which utilizes the change in resonant wavelength to determine the value of analyte whereas, the amplitude interrogation technique is intensity-based, which utilizes the difference in the modal loss for the determination of the analyte. However, the use of a power meter and the unnecessary use of wavelength interpolation results in the amplitude interrogation method being comparatively less complicated, simple, and cost-effective at the same time. Amplitude susceptivity can be determined while using the following calculation [86]:

$$S_A(\lambda)[\mathrm{RIU}^{-1}] = -\frac{1}{\alpha(\lambda, \mathrm{n}_a)} \frac{\partial \alpha(\lambda, \mathrm{n}_a)}{\partial n_a} \tag{4}$$

Here, $\alpha(\lambda, \mathrm{n}_a)$ implies confinement loss at analyte RI, n_a, $\partial\alpha(\lambda, \mathrm{n}_a)$ implies the confinement loss dissimilarity between two successive analyte refractive indexes in a row. In fact, amplitude interrogation technique is quite exposed to disturbances, which makes wavelength technique comparatively more responsive towards sensitivity. Sensitivity is obtained in the wavelength interrogation method using the following equation [87]

$$S_{\lambda}(\lambda)[\mathrm{nm/RIU}] = \Delta\lambda_{peak} / \Delta n_{a} \tag{5}$$

Here, $\Delta\lambda_{peak}$ is clearly the change in peak wavelength, Δn_{a} denoting the shift in two successive RI. Sensor Resolution plays a very significant role in disclosing the analyte RI variation. However, this sensor determination of a surface plasmon resonance is enhanced as the linewidth of the SPR indicating dip reduces, and the variation in the resonance shift increases. Sensor resolution is determined by the following calculation [74]:

$$R(\mathrm{RIU}) = \mathrm{n}_{a} \times \Delta\lambda_{\min} / \Delta\lambda_{peak} \tag{6}$$

Where, $\lambda_{\min}$ is the least wavelength resolution. Besides the sensitivity as well as sensor resolution of a PCF- based sensor, Sensor length is an important parameter as well. The target goal of this paper is to present a design that allows its required transferred signal to maintain its undeviating polarization alongside the sensor length. Sensor length is specified by the following calculation [88]:

$$L = \frac{1}{\alpha(\lambda, \mathrm{n}_{a})} \tag{7}$$

4.4 Simulation Results

All geometrical parameters have a substantial impact over the performance of sensing. The phase-complementing points are assorted by altering parameters like thickness of gold (Au) layer, sensing/analyte layer, PML thickness, and pitch.

Gold thickness plays a significant role in shifting the resonance wavelength resulting in affecting the performance evaluation of the sensor. An increment in gold thickness results in shifting the resonance wavelength to longer wavelengths. Maintaining a suitable range of lambda from 650nm to 820nm, we note that amplitude sensitivity increases progressively with the increment in the plasmonic layer thickness starting from 30nm to 35nm. Sensitivity reduces for 30nm gold thickness because of the limitation called skin depth of surface plasmons [72]. However, sensitivity ceases to decrease with further increment in Au thickness from 35 nm to 40 nm as it becomes very difficult for evanescent field to penetrate the gold layer and interplay the sensing layer [78], and thus, sensitivity peak 780.7 RIU^{-1} is obtained when the gold thickness is 35 nm. Thus, we optimize the layer at this point. Table 5.1 displays amplitude sensitivity variation with the alteration of gold thickness. Fig. 4.3 (a, b) illustrates the attaining of variation in gold thickness in x-polarization mode on the sensing performance.

Table 4.1
AS variation with the alteration of gold layer thickness

Gold	Analyte RI	Peak Loss(dB/cm)	Wavelength Sensitivity(nm/RIU)	Amplitude Sensitivity (RIU^{-1})
30nm	1.38 1.39	45.28 50.15	4000	504.57
35nm	1.38 1.39	76.59 108.58	5000	780.07
40nm	1.38 1.39	54.28 95.62	3000	563.35

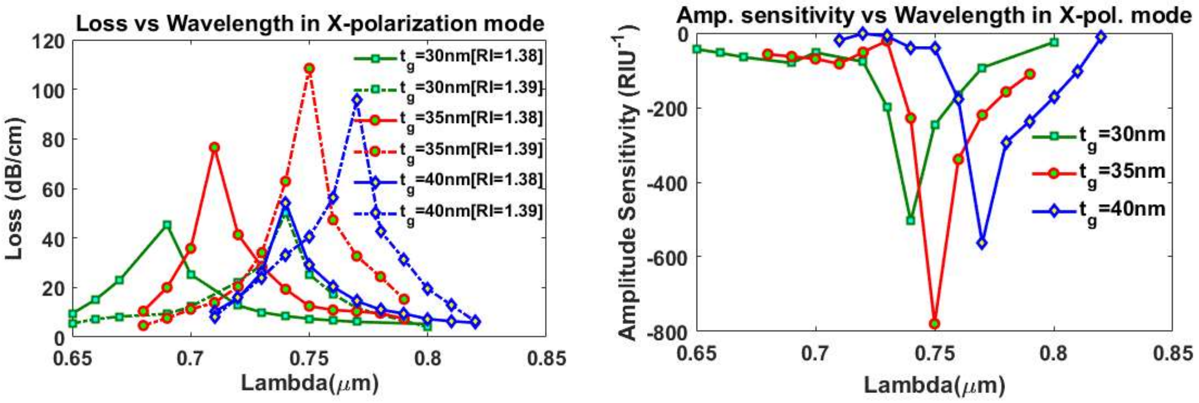

(a) (b)

Figure 4.3: Variation in CL and AS due to gold thickness for analyte refractive index η_a = 1.38 and 1.39

Fig. 4.4 (a, b) reflects the effect on sensitivity due to variance in the sensing layer, although the change is not that noteworthy. Keeping gold thickness 35nm, the sensing layer has been changed and maximum sensitivity 881.2 RIU^{-1} is obtained for 0.82µm. Table 4.2 displays performance comparison for different sensing layer lengths. The peak loss increases with the increasing value of analyte [78]. Unfortunately, an increase in peak loss limits the value of sensitivity [89]. Initially, the sensitivity increased for an increase of analyte from 0.81µm to 0.82 µm. However, with the increasing value of analyte from 0.82µm to 0.85µm the peak loss increases simultaneously resulting in the drop of sensitivity. Thus, maximum amplitude sensitivity is obtained for 0.82 µm.

Table 4.2

AS variation with the alternation of sensing medium layer

Analyte	Analyte RI	Peak Loss(dB/cm)	Wavelength Sensitivity(nm/RIU)	Amplitude Sensitivity (RIU^{-1})
0.81µm	1.38 1.39	51.5 52.6	6000	858.5
0.82µm	1.38 1.39	50.7 55.42	6000	881.2
0.85µm	1.38 1.39	49.5 60.36	6000	877.89

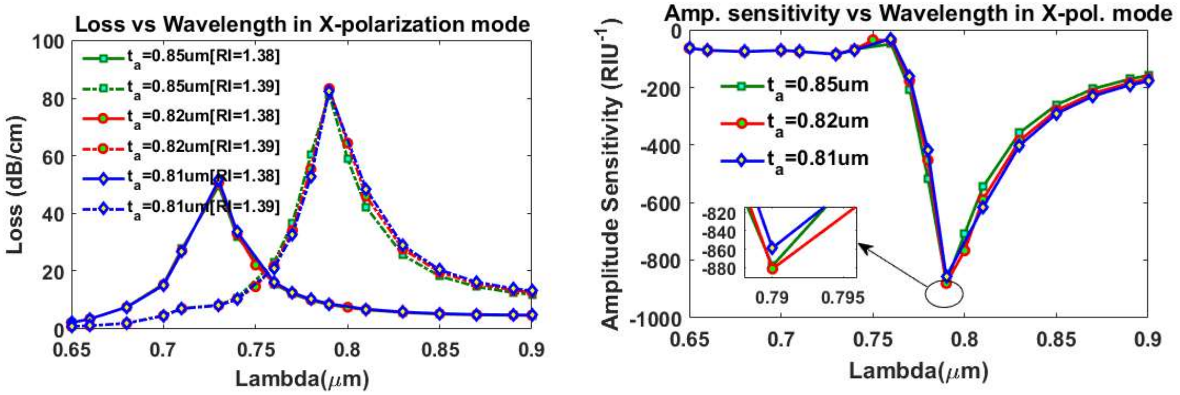

(a) (b)

Figure 4.4: Variation in CL and AS due to change in analyte thickness (sensing length) at analyte refractive index η_a = 1.38 and 1.39

The flawlessly suited layer is used to assimilate radiation towards the surface. Although the effect of the thickness of PML is not significantly large on the sensitivity of the sensor, but the thickness should be such that it can absorb the radiation successfully. Fig. 4.5 (a, b) shows confinement loss and sensitivity of the offered sensor for different perfectly matched layer (PML) depth. Keeping gold thickness 35 nm and sensing length 0.82 µm, we changed PML thickness and acquired the following variation in peak loss and sensitivity in Table 4.3.

Table 4.3

AS variation with the alteration of PML layer

PML Depth	Analyte RI	Peak Loss(dB/cm)	Wavelength Sensitivity(nm/RIU)	Amplitude Sensitivity (RIU^{-1})
1.18µm	1.38 1.39	55.22 82.01	8000	1022.9
1.20µm	1.38 1.39	56.25 84.51	8000	1032.9
1.22µm	1.38 1.39	57.54 82.375	8000	975.3

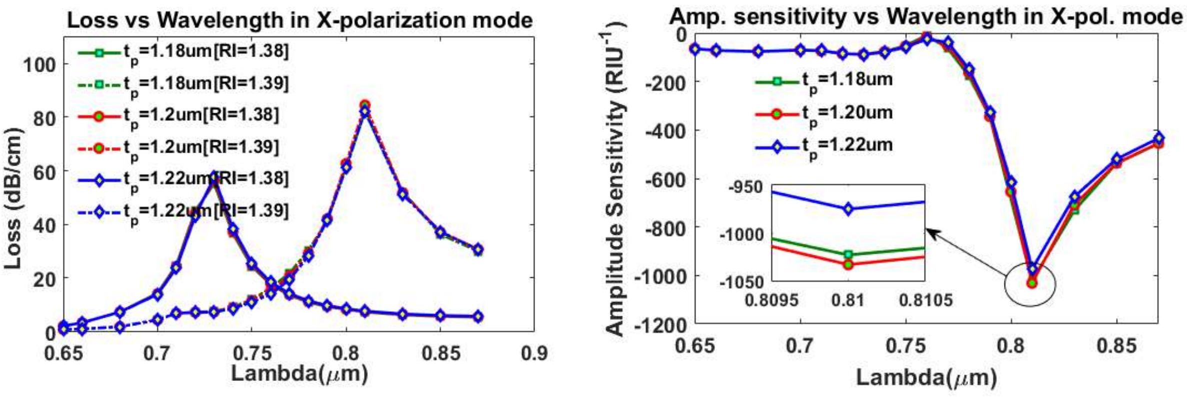

(a) (b)

Figure 4.5: Variation in confinement loss and amplitude sensitivity due to change in PML depth at analyte refractive index η_a = 1.38 and 1.39

Even though the confinement loss is quite similar, we obtained improved sensitivity of 1032.9 RIU^{-1} for PML depth of 1.20µm.

To increase sensor performance further the diameter of cladding air holes is investigated. Fig. 4.6 (a, b) shows the change in confinement loss and in sensitivity due to change in center/large air holes. A peak sensitivity of 1244.1 RIU^{-1} is obtained for a diameter of 1.96µm. When diameter is changed from 1.96µm to 1.92µm, the distance between center four air holes increases and thus evanescent field spreads over the channel between air holes. This causes less excitation of surface plasmons and in return amplitude sensitivity decreases [82]. But when diameter is increased to 2µm, the distance between center air holes decreases, making less guiding light towards the metal-dielectric interface and more towards the core and therefore amplitude sensitivity decreases for 2 µm diameter [82]. Table 4.4 shows the variation in different parameters:

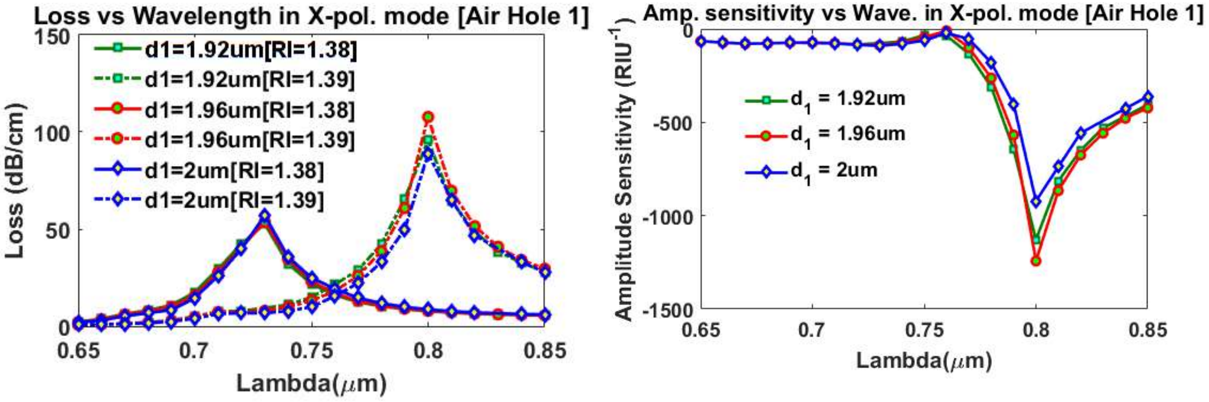

(a) (b)

Figure 4.6: Variation in confinement loss and amplitude sensitivity due to change in diameter of center/large air holes at analyte refractive index η_a = 1.38 and 1.39

Table 4.4

Amplitude sensitivity variation with the alteration of diameter of center/large air holes

Diameter of cladding air hole	Analyte RI	Peak Loss (dB/cm)	Wavelength Sensitivity (nm/RIU)	Amplitude Sensitivity (RIU^{-1})
1.92µm	1.38 1.39	52.69 95.73	7000	1129.3
1.96µm	1.38 1.39	53.71 107.70	7000	1244.1
2µm	1.38 1.39	57.01 88.81	7000	922.26

Effective excitation of the surface the metal is the core driver to the plasmonic phenomenon. At a particular wavelength, the incident light generates surface plasmon resonance. In this suggested design, initially, the diameter of the extra two air holes is kept 0.6µm. Diameters smaller than this will cause a reduction in surface excitation, which is not acceptable. However, if the diameter is increased, the core-guided effective index will reduce along with the surface excitation [82]. Fig. 4.7 (a, b) is displaying the result on sensitivity due to variation in the extra air holes diameter in the cladding region.

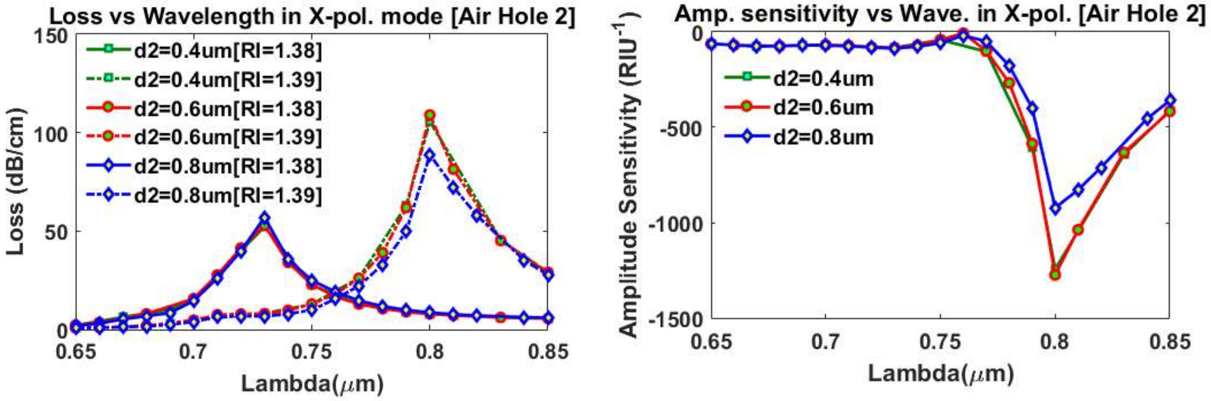

(a) (b)

Figure 4.7: Variation in confinement loss and amplitude sensitivity due to change in diameter of extra/small air holes at analyte refractive index η_a = 1.38 and 1.39

Table 4.5

Amplitude sensitivity variation with the alteration of diameter of extra/small two air holes

Diameter	Analyte RI	Peak Loss(dB/cm)	Wavelength Sensitivity (nm/RIU)	Amplitude Sensitivity (RIU^{-1})
0.4µm	1.38 1.39	52.18 63.04	7000	1244.4
0.6µm	1.38 1.39	52.95 61.90	7000	1273.5
0.8µm	1.38 1.39	57.01 88.81	7000	922.26

From Table 4.5, utmost amplitude sensitivity of 1273.5 RIU^{-1} and wavelength sensitivity of 7000 nm/RIU is achieved considering a diameter of 0.6µm.

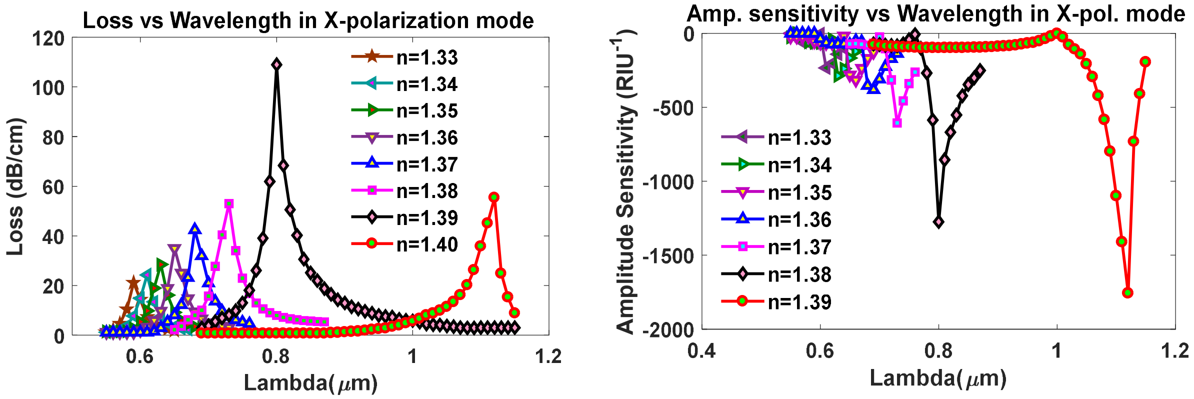

(a) (b)

Figure 4.8: Variation in confinement loss and sensitivity in analyte RI range of 1.33-1.39

Investigation of the proposed sensor is done by measuring confinement loss characteristics of various analytes. From Fig. 4.8 (a), we can observe that resonance peak retracts approaching longer wavelengths as analyte RI is increased. Besides, it changes RI of plasmonic mode that eventually alters the phase-matching points. The span of analyte RI is taken from 1.33 to 1.40, considering practical biochemical interactions. Fig. 4.8 (b) demonstrates the sensitivity which is increasing with the increment of the resonance peak. Table 4.6 demonstrates the characteristics of the proposed sensor for a wide range RI of the analyte for x-polarization mode.

Table 4.6

Performance Analysis by altering analyte refractive index (1.33 to 1.40)

Analyte RI	Peak loss (dB/cm)	Res. peak wavelength (nm)	Res. peak shift(nm)	Amplitude Sensitivity (RIU^{-1})	Wavelength Sensitivity (nm/RIU)	Sensor Resolution	FOM
1.33	21.14	590	20	233.56	2000	5×10^{-5}	189.2
1.34	24.28	610	20	286.62	2000	5×10^{-5}	164.7
1.35	28.43	630	20	315.778	2000	5×10^{-5}	140.7
1.36	34.99	650	20	380.93	3000	5×10^{-5}	207.0
1.37	42.42	680	30	605.84	5000	3.33×10^{-5}	235.7
1.38	52.95	730	50	1273.5	7000	2×10^{-5}	264.4
1.39	108.99	800	70	1757.3	32000	1.428×10^{-6}	587.2
1.40	55.35	-	-	N/A	N/A	N/A	N/A

From the table, we can see maximal value of AS and WS is 1757.3 RIU^{-1} and 32,000 nm/RIU respectively. Also, we obtained a sensor resolution of 1.428×10^{-6} that implies the degree of detection for minimum change in lambda of 0.1 nm.

The figure of merit is the ratio between the sensitivity and the full width at half maximum (FWHM) for evaluating the performance of an SPR sensor, which can be described as follows: [75]

$$FOM = \frac{Sensitivity}{FWHM}(\mathrm{RIU}^{-1}) \tag{8}$$

In general, FOM points out the quality performance of any device. For maintaining an overall higher sensing performance, it is required to maintain the figure of merit as high as possible. An expansion in sensitivity and reduction in FWHM simultaneously brings about the accretion of FOM. Again, for a plasmon sensor, the critical parameter of high FOM indicates high sensitivity and high wavelength resolution. Still, the figure of merit can be intensified with a silica film of lower refractive index [90]. Performance improvement in the sensor validates the improvement of FOM. For the proposed design, maximum FOM obtained is 587.2.

Birefringence is another property of a PCF-SPR sensor as it increases the sensitivity and shows different sensitivity for x- and y-polarized mode signals. The input (linearly polarized light) launched on the axis (x or y) of the fiber preserves the polarization state throughout the optical fiber length which is independent of exterior mechanical; also any thermal agitations. In addition, a birefringent fiber is essential for signal reception when it is launched in either x or y-polarization axis. By choosing the input signal, we can select on axis for improving the fiber sensitivity and the other axis for reducing the loss [76]. Also, birefringence shows the coupling efficiency of a fiber. It can be calculated using: [91, 92]

$$B = \left| n_x - n_y \right| \tag{9}$$

Here, n_x denotes EMI in the x-pol. and n_y denotes the EMI in y-pol. respectively. Generally, circular or solid core fibers show almost zero birefringence. For simplicity of fabrication and practical implementation, we use circular symmetrical air-holes thus we obtained birefringence of 0.0004 RIU, which is a promising trade-off between structural complexity and sensitivity.

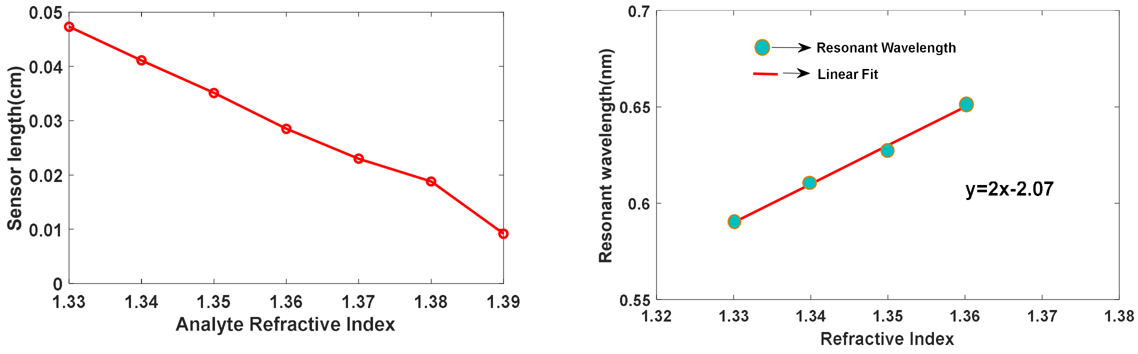

(a) (b)

Figure 4.9: (a) Change in sensor length with increment of analyte RI; (b) Regression line for resonance wavelength variation with analyte Refractive Index

Fig. 4.9 (a) shows the variation in sensor length compared to different analyte RI. Sensor length diminishes with the augmentation of the analyte refractive index as it completely depends on absorption loss. From the figure, we can say, the possibility of the use of sensing length of a few millimeters to centimeters to detect unidentified analytes is possible.

Assessment of sensors for particularly higher RI analytes requires high linear fitting characteristics [88]. Generally, high linearity is desirable as it is an indication of a high-quality sensor. In this case, the linear fit is an essential parameter necessary for the optimization of the sensor. To avoid the complexity of the detection process, the non-linear fitting characteristic is not preferable. However, the slope of the curve usually points out the mean sensitivity of a PCF- based sensor, which is somewhat disrupted by the non-linear fitting property [49]. Fig.4.9 (b) illustrates that the proposed sensor shows a linearly fitted curve with a R^2 value of 0.998. The linear regression line equation is $y = 2x - 2.07$, where, x,y denotes the refractive index of the analyte, resonance wavelength, respectively.

4.5 Fabrication Tolerance

The fabrication tolerance for the design has been investigated as given in the Fig. 4.10. As during fabrication, the exact measurements for the parameters are impossible to maintain so we have considered ±10% variation from the optimized value in the parameters to see if the fabrication is still acceptable with such variations. The gold thickness is optimized at 35 nm which is shown in Fig. 4.10 (a). Gold layer thickness exhibits huge influence on sensitivity and loss depth [93]. A thin gold layer shows higher loss depth and sensitivity [94]. Due to ±10% variation in the gold layer thickness, the variation observed in loss depth and sensitivity is negligible compared to that of the optimum value.

The analyte has been optimized at 0.82μm and considering the variations, the resonant wavelength remains within ±2% of the optimized value which has been shown in Fig. 4.10 (b). Though, loss depth is changed moderately yet the resonant wavelength variation is negligible where we concluded to keep the analyte optimized value at 0.82μm.

In the case of PML shown in Fig. 4.10 (c), the optimized value obtained is at 1.2µm and for the variations, the resonant wavelength remains within ±5% of the optimized value. The mirroring of the light-penetration from PCF is absorbed depending on the PML thickness [75]. PML thickness difference of 10% marginally altered imaginary part of Effective-Index (EI) which results in small variation in loss depth. However, the resonant wavelength variation remains negligible which exhibits unaltered sensor performance.

The diameter of the smaller circles (d_2) has significant dominance over the sensing execution by signifying phase-matching phenomena. The smaller hole diameters have been optimized at $d_2 = 0.6$ µm; if it is decreased gradually, the EI of core guided mode becomes low. As a result, controlling light seems to disseminate towards cladding region, which results in higher confinement loss and prevents the practical realization. But when the value is increased, the light will be more gathered towards the core however surface excitation is given more priority for SPR [78]. The variations of d_2 show contrast in loss depth. The increment in d_2 conveys decrease in loss depth while decreasing it shows drastic reduction of loss depth. The resonant wavelength of the variations remains within ±3% of the optimized value for d_2 shown in Fig. 4.10 (d).

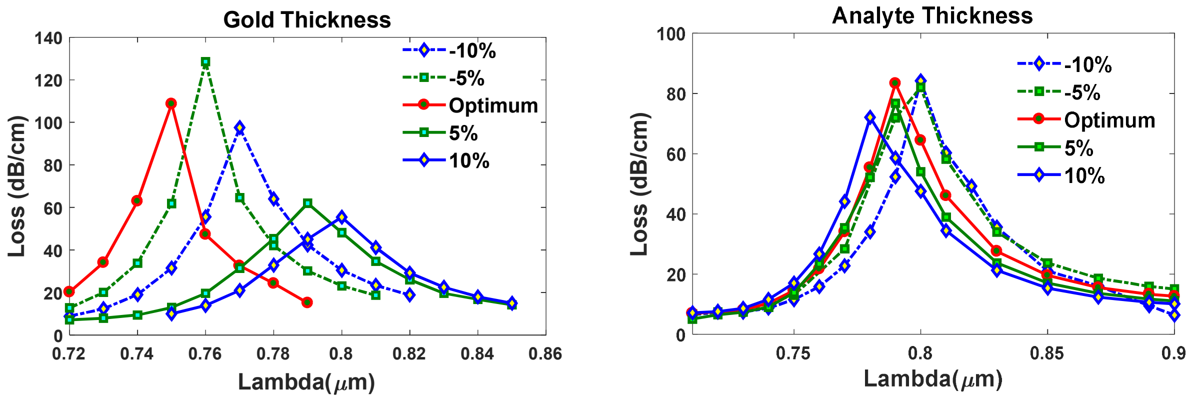

(a) (b)

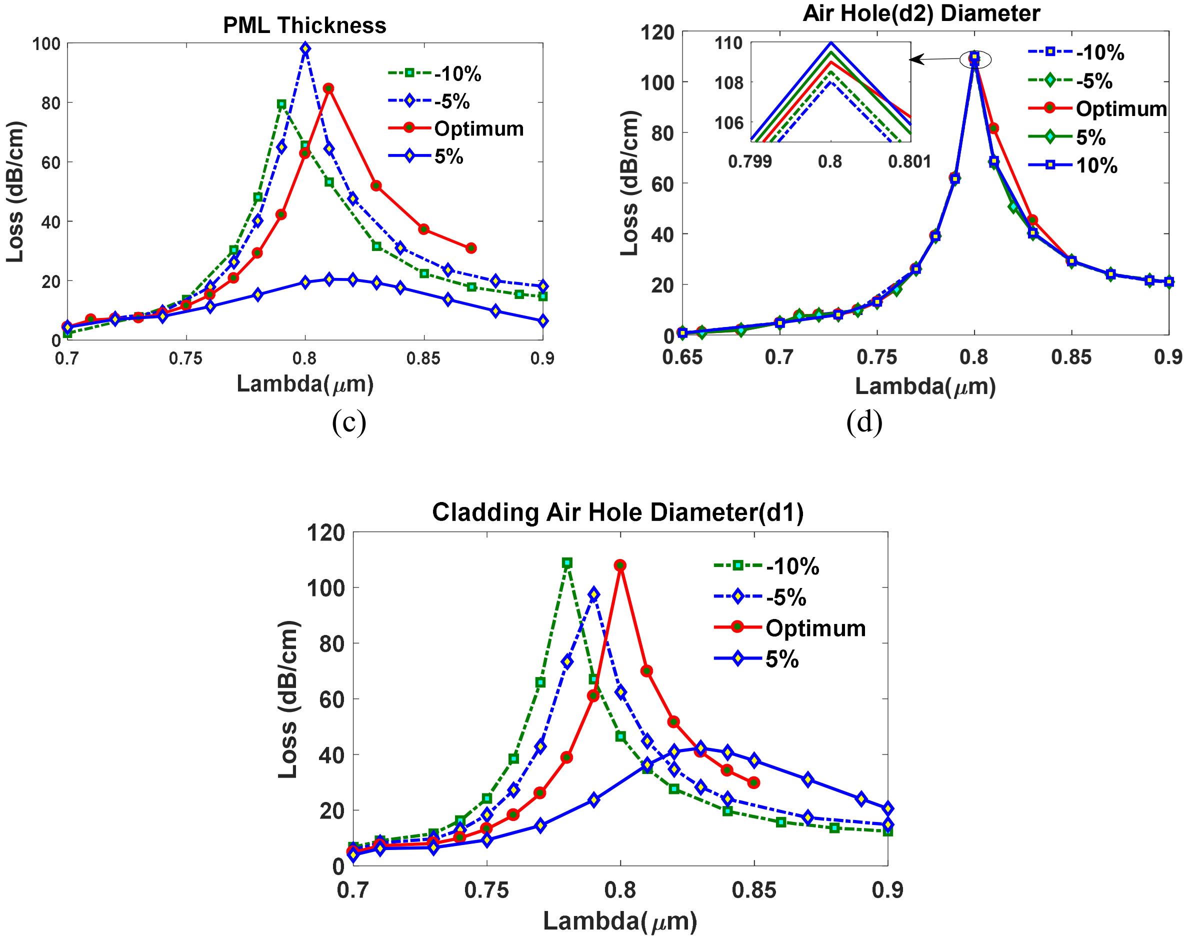

(c) (d)

(e)

Figure 4.10: Loss spectrums for variation in (a) gold layer thickness, (b) analyte thickness, (c) PML thickness, (d) diameter of cladding air hole, and (e) diameter of small air hole for x-polarized mode.

Considering the cladding air holes, the optimization is seen at d_1= 1.96µm shown in Fig.4.10 (e). The variation in d_1 exhibits an opposite effect on the sensing compared to d_1 [78]. However, the loss for variation is negligible but the resonant wavelength shifts a bit. Increasing diameter of larger air holes by 5%, decreases the loss spectrum. As the resonant wavelength remains in a close range, so it does not seem to have effect over fabrication. From investigating the fabrication tolerance, it is noticed that while varying the parameters ±10%, there is change in the loss depth, the resonant wavelength remains fairly the same. So, sensing performance will not be hampered after fabrication. Since the structure is simple, the offered PCF has the potential to be implemented practically after being fabricated by the method termed as Stack-and-Draw [95]. The thin gold layer is placed by Chemical Vapor Deposition as well as sputtering techniques as they are the most common methods to coat PCF structures [96]. Also considering recent advancement, Atomic Layer Deposition (ALD) is another technique for gold-layer coating [97].

The fabrication of the proposed sensor is actually pretty straight forward. We can see only circular shaped airholes are used in this sensor and the number of airholes is only four. And this makes it extremely easy to fabricate in the most popular fabrication technique named "Stack and draw method". D. Pysz. et al. described the whole process in detail in their paper [98]. The whole process is described below:

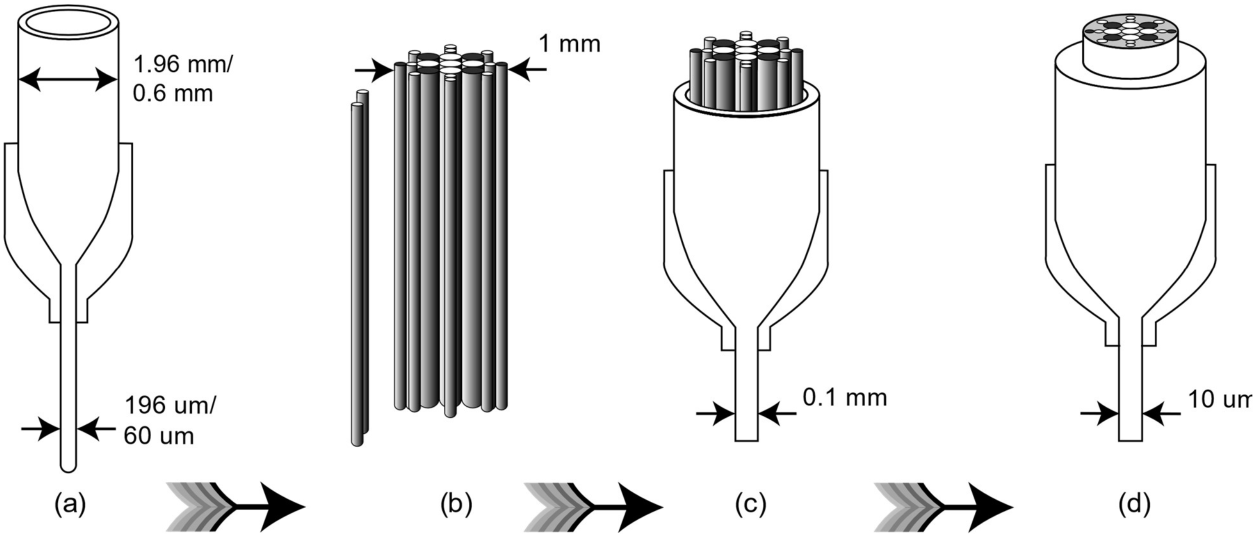

Fig 4.11: Step by step fabrication of the proposed fiber in stack and draw method (capillary stacking process)

As we can see, from fig 4.11(a) at first two types of capillaries are created. These capillaries are much greater in size than the actual capillaries. Normally the size is 100times than the actual size. So, 100 times greater than the two types of airholes (1.96 µm and 0.6µm) are 196µm and 60µm in diameter.

Then a preform is created stacking all the capillaries like fig 4.11(b). Then with the help of a screw and holder the entire preform is run through a furnace and drawn downwards. With the help of a diameter monitor, the size of the cane is maintained to be 10 times lesser than the whole stack. So, in the cane the size of airholes become 19.6μm and 6μm. Then this cane also goes through a furnace which then makes the size of the airhoes to 1.96μm and 0.6μm.

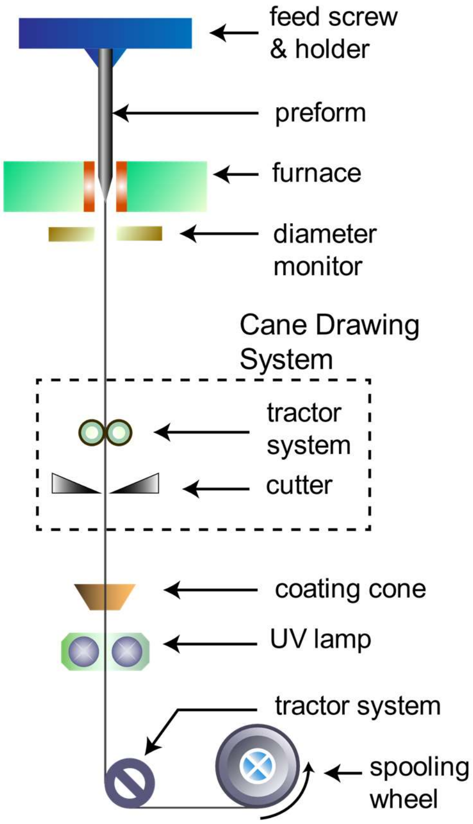
feed screw
& holder
preform
furnace
diameter
monitor
Cane Drawing
System
tractor
system
cutter
coating cone
UV lamp
tractor system
spooling
wheel

Fig 5.12: Step by step fabrication of the sensor (Drawing process)

As we have already mentioned, using this process the size of the airholes can be taken down to much smaller than what we have proposed without any deformation.

Table 4.7
Comparative analysis of the suggested sensor and prior stated sensors

Ref.	RI range	Max. Amplitude Sensitivity (RIU^{-1})	Max. Wavelength Sensitivity (nm/RIU)	Sensor Resolution	FOM	Birefringence
88.	1.46-1.485	820	23000	4.35×10^{-6}	-	-
93.	1.33-1.37	860	5000	4×10^{-5}	-	-
94.	1.18-1.36	1054	20000	5×10^{-6}	250	-
95.	1.33-1.43	1086	44000	2.2×10^{-6}	502	1.6×10^{-3}
74.	1.36-1.41	1222	14660	6.82×10^{-6}	1140	1.2×10^{-3}
96.	1.33-1.38	1411	25000	4×10^{-6}	-	-
97.	1.33-1.43	1415	6200	1.61×10^{-6}	-	-
98.	1.33-1.39	1506	22000	6.64×10^{-6}	508	-
This paper	1.33-1.39	1757.3	32000	1.428×10^{-6}	587.2	4×10^{-4}

4.5 Discussion

A simple single-layer square lattice plasmonic PCF biosensor is proposed here with external sensing operability. The objective of this research is to put forward draft based wholly on annular air holes. We have considered all structural parameters to attain the maximum sensitivity and sensor resolution possible. Table 5.7 depicts the comparison between the proposed biosensor and previously reported sensors. The proposed sensor offers highest amplitude sensitivity of 1757.3 RIU^{-1} and highest wavelength sensitivity of 32000 nm/RIU. Sensor resolution of 1.428×10^{-6}, FOM of 587.2, and birefringence of 0.004 RIU is obtained for x-polarization, which means it can ascertain very little alteration in the analyte. Moreover, small sensor length is required, and fabrication can also be done using the usual Stack and Draw method. Moreover, using CVD (chemical vapor deposition) method plasmonic gold layer can be placed on the structure to alleviate fabrication and making it practically manufacturable. Due to improved modal properties with a simple structure, this proposed sensor can be implemented in numerous real-time diagnostic studies in biomedical, biochemical applications.

Chapter 5: Modeling and Numerical Analysis of PCF Biosensor Using Single Hexagonal Lattice Structure

5.1 Introduction

PCF based SPR sensor method is the fusion of photonic crystal fiber-based technology in the field of plasmonic science [99]. However, a prism based sensor is readily available and economically affordable, but its constraints are heavyweight and unsuited for remote sensing [57]. However, SPR sensor is well-known for its design flexibility and comparatively small structures, and controllable birefringence [76]. The performance a SPR biosensor is highly influenced by plasmonic materials. Usually, gold and silver have extensively been utilized to make the SPR biosensor [100]. Silver provides precise resonance peak as a sensor material in comparison with other materials. However, due to its highly conductive nature, silver gets oxidized very quickly and creates a hindrance for the sensor performance [60]. As a sensor material, gold is more advantageous because of the inert nature and for being able to provide a comparatively larger resonance wavelength shift [101]. In reference to the prospects, different plasmonic structures like square, hexagonal, hybrid octagonal, etc. can control core-guided propagation. Furthermore, the optimized value of structural parameters can manipulate the guiding behavior [58, 59].Usually, almost every disclosed PCF SPR sensors show only one of two polarization modes is comparatively more robust than the other. But, both of the x and y-polarization modes can also demonstrate coupling at the same wavelength [102]. The standard plasmonic SPR sensing technology is relying on the operational mechanism of Kretschmann and Reathers [103]. According to some recent research, the internal sensing mechanism is used more for obtaining precise values [104, 105, 66]. Nevertheless, the internal sensing methodology is disadvantageous for some real-time implementations. Fiber optic SPR biosensors bear the characteristics of scaling down, a much higher degree of incorporation, and acute sensing capacity[106], [107].These unique properties of PCF sensors have managed to secure their position in signal processing system and optical communication [108],[84]. The proposing structure assimilates a single layer of hexagonal shaped lattice configuration and a layer of plasmonic material. Air holes are provided for light guidance. With the aim of diminishing the propagation losses between the core guided mode and plasma mode extra small air holes are integrated between the central air holes. The proposed structure has the potential to get manufactured without difficulty as it made up of only circular shaped air holes.

5.2 Proposed Structure and Theoretical Analysis

This design (Figure 5.1) includes annular air holes laid out in a hexagonal grid. Additional small circular shaped hole is placed at the center. The air holes work as a low refractive index in the cladding region allowing the fiber core to be mode guidance friendly. Opposite small air holes from both sides are eliminated to ensure a balanced drift to the evanescent field. The analyte layer serves as a sensing medium, and its thickness is selected based on the convergence test. For the background material we have chosen fused silica (SiO_2), and its refractive index is wavelength dependent.

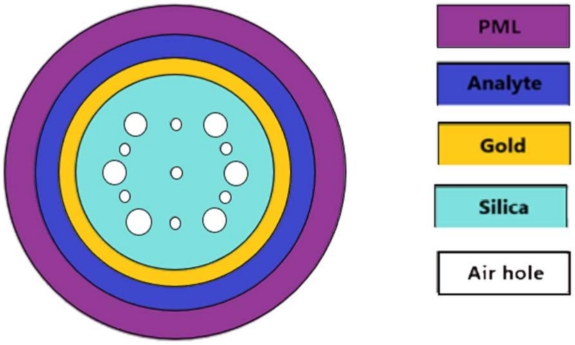

Figure 5.1: Cross sectional 2D view of the proposed fiber

It can be calculated by Sellmeier equation as stated before

$$n^2(\lambda) = 1 + \frac{B_1\lambda^2}{\lambda^2 - C_1} - \frac{B_2\lambda^2}{\lambda^2 - C_2} - \frac{B_3\lambda^2}{\lambda^2 - C_3} \quad (1)$$

Here, *n* is refractive index, wavelength in vacuum of fused silica is denoted by *λ* (μm). Sellmeier Coefficients are $B_1 = 0.696163$, $B_2 = 0.4079426$, $B_3 = 0.8974794$, $C_1 = 4.679148 \times 10^{-3}$ μm^2, $C_2 = 1.351206 \times 10^{-2}$ μm^2 and $C_3 = 97.93400$ μm^2.

The computational domain subdivided the structure into 20992 triangle elements, 1716 edge elements with minimum element quality of 0.3374, average element quality of 0.8055, element area ratio of 0.002123, and mesh area of 163.2μm^2.

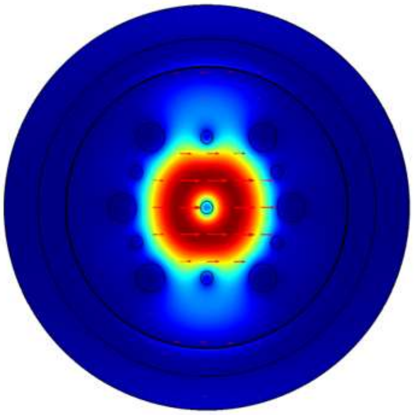

(a)

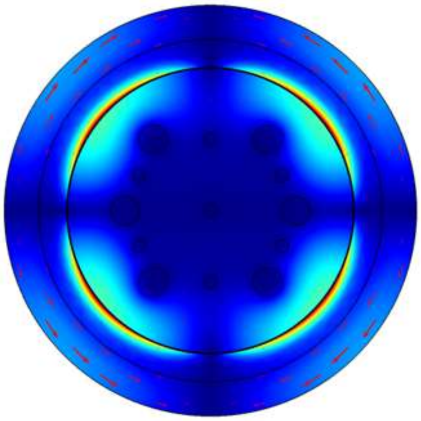

(b)

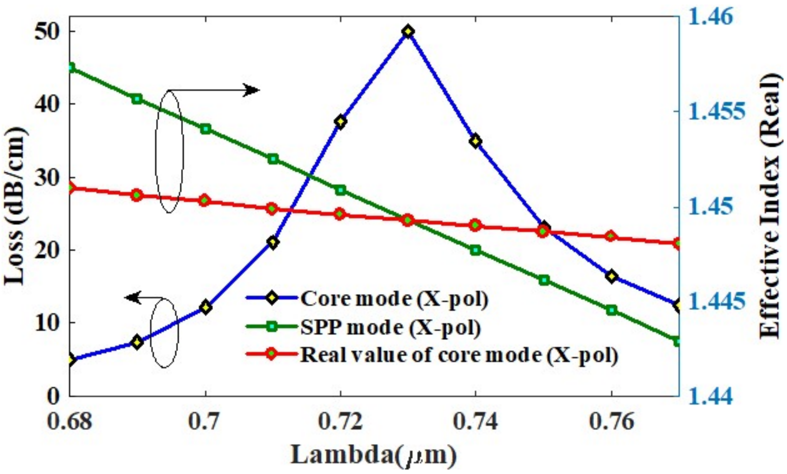

Figure 5.2: (a) Core-guided mode and (b) SPP mode for x-polarization (c) Dispersion between fundamental mode and SPP mode

From fig. 5.2 (a) shows the core-guided mode and fig 5.2 (b) demonstrates SPP mode. The main prerequisite for surface plasmon resonance is to have a metal dielectric interface where light matter interaction happens. The gold layer provides the metal-dielectric interface that is required to generate SPR. The plasmonic layer is the most essential part of this study as gold layer supplies surface plasmons which are essential for surface plasmon resonance. The figure 5.2(c) shows the dispersion relation at analyte RI of 1.38. The loss shown here is caused by a number of reasons such as the airhole diameter, gold layer thickness, airhole distribution etc. The guiding property of the sensor is mainly responsible for this loss. If less light is guided through the core and more through the cladding region, then the loss is high. But if more light is guided through the center and less through the cladding region, then the fiber becomes less lossy. In this case fiber also becomes less sensitive. That is why optimization of this type of sensor is needed in order to ensure and select the best results in terms of loss and sensitivity. Thereby at that particular point, confinement loss of core mode is obtained maximum. We can determine the confinement loss (CL) through the following formula

$$\alpha = 40\pi.\mathrm{Im}(\mathrm{n}_{eff})/(\ln(10)\lambda) \approx 8.686\times k_0.\mathrm{Im}[\mathrm{n}_{eff}]\times 10^4\, dB/cm \tag{3}$$

where the wavenumber is denoted by k_0 is and it can be solved by $k_0 = 2\pi/\lambda$. Here λ connotes the working wavelength and Im (n_{eff}) entitles the imaginary part of n_{eff} . ε_{Au} can be obtained from the Drude-Lorentz equation [84].

$$\varepsilon_{Au} = \varepsilon_{\infty} - \frac{\omega_D^2}{\omega(\omega + j\gamma_D)} - \frac{\Delta\varepsilon.\Omega_L^2}{(\omega^2 - \Omega_L^2) + j\Gamma_L\omega} \tag{2}$$

Where, the permittivity of gold is indicated by ε_{Au} , ε_{α} signifies permittivity for higher value of permittivity and value is 5.9673, ω is the angular frequency calculated by $\omega=2\pi c/\lambda$. Here, γ_D represents damping frequency, ω_D represents the plasmon frequency and $\gamma_D/2\pi=15.92THz$, $\omega_D/2\pi=2113.6\ THz$, $\Omega_L=650.07THz$ and the spectral width is $\Gamma_L/2\pi=104.86THz$.

When analyte refractive index is shifted the value of loss also gets changed. This phenomenon is implemented for the detection of unidentified analytes. This is known as amplitude interrogation. It can be estimated using [77, 33]:

$$S_A = -\frac{1}{\alpha(\lambda, n_a)} \frac{\partial \alpha(\lambda, n_a)}{\partial n_a} (RIU^{-1}) \tag{4}$$

Where α (λ, n_a) signifies the confinement loss of the analyte at a precise RI and $\partial\alpha(\lambda, n_a)$ is the confinement loss difference of two successive analyte RIs.

Wavelength interrogation is another spectral-based measurement technique to identify analyte. In this case the shift of resonant wavelength is examined. The performance of a sensor can be assessed by both amplitude sensitivity and wavelength sensitivity. Conventionally wavelength interrogation is more prone to sensitivity than amplitude interrogation method. Hence high sensitivity response is achieved from this technique [75]. The formula stated below is used to calculate the sensitivity of a sensor [77]:

$$S_\lambda = \Delta\lambda_{peak} / \Delta n_a (nm / RIU) \tag{5}$$

Here $\Delta\lambda_{peak}$ symbolizes the maximum resonant wavelength shift and Δn_a implies the difference between two sequential analytes RI.

Sensor resolution is a crucial parameter that shows the smallest amount of change a sensor can detect. It is estimated by the succeeding equation [77]:

$$R = \frac{\partial n_a \times \partial \lambda_{\min}}{\partial \lambda_{peak}} (RIU) \tag{6}$$

Here, the terms $\partial\lambda_{min}$ and $\partial\lambda_{peak}$ signify the least spectral resolution and resonant λ shift, respectively. Birefringence is a parameter that is used to show the coupling efficiency of a fiber.

$$B = \left| n_x - n_y \right| \tag{7}$$

Using this equation birefringence can be calculated. Here, n_x and n_y denotes the effective mode index (EMI) in the x and y pol. respectively.

5.3 Numerical Analysis and Discussion

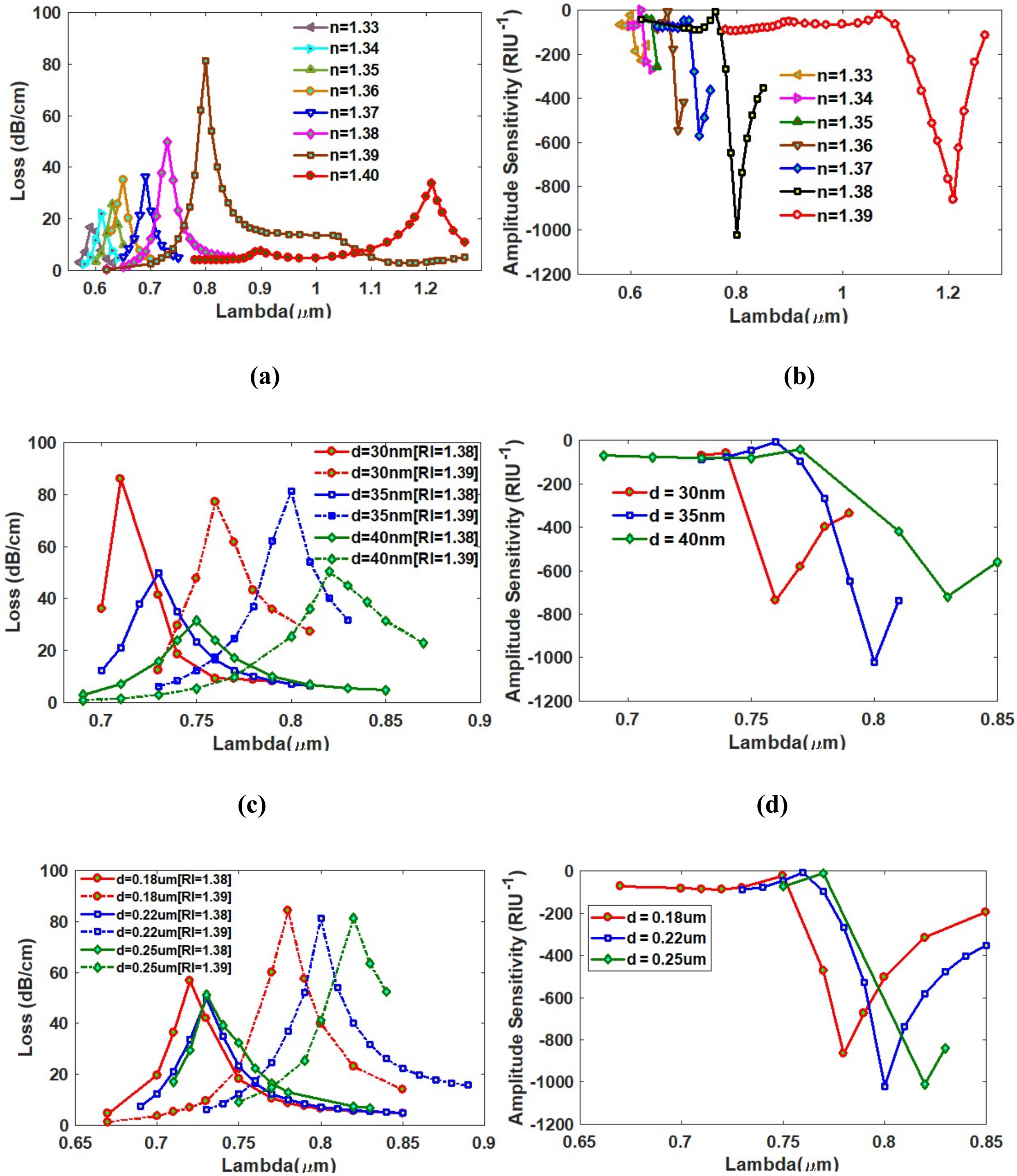

(a)

(b)

(c)

(d)

(e) **(f)**

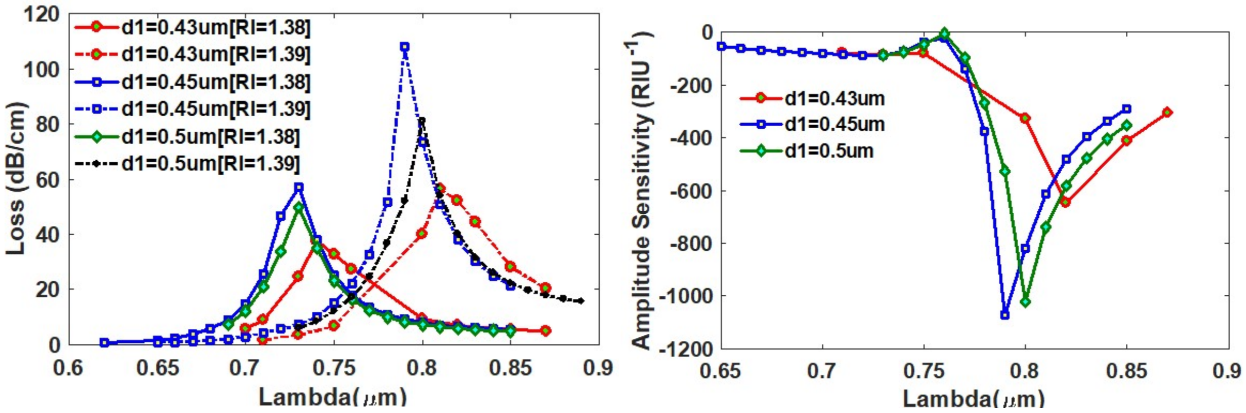

(g) **(h)**

Figure 5.3: CL versus AS due to change in (a,b) analyte RI from 1.33 to 1.40, (c,d) gold thickness (e,f) diameter of small air holes, and(g,h) diameter of air holes in the cladding region

From figure 5.3(a), we can observe that resonance peak gradually shifts towards higher value of wavelengths with analyte RI. The range of analyte RI starts from 1.33 to 1.40. From figure 5.3(b) we can see the sensitivity of the proposed design. Evaluation of sensors for significantly higher RI analytes requires high linear fitting characteristics. The highest AS is obtained at RI of 1.38, which was kept constant throughout the analysis of all other parameters. The analysis is started by investing the gold layer. Gold of thickness of 30nm, 35nm, and 40nm were taken, where the obtained amplitude sensitivities were 770.3, 1021.7, and 1001.2, respectively for the refractive indexes of 1.38. So, the optimized value for gold thickness is 35nm, and the rest of the parameters were investigated to keep this constant. Next, the smaller air-slot diameter was taken into account, being 0.18 μm, 0.22 μm, and 0.25 μm with amplitude sensitivities of 866.4, 1021.7, and 1011.8, respectively. This shows the smaller air slot optimized radius was at 0.22 μm, and the rest of the simulation was done keeping this value fixed. Finally, the larger air hole radius was considered at 0.43μm, 0.45μm and 0.5μm with amplitude sensitivities of 775.83, 1037.4 and 1021.7, respectively for refractive indexes of 1.38. In practical implementation or in practical situation the thickness of the analyte layer should be such that it doesn't let PML layer to influence guiding properties. That is why the layer thickness should be a variable one. In our paper, we have optimized the analyte layer to get the maximum possible results (amplitude sensitivity and wavelength sensitivity). The analyte and PML thickness were optimized at 0.98 μm and 1.2 μm, respectively. In practical realization the thickness should be changed based on the airhole diameter, gold thickness etc. That is why we have made a visual illustration of how the system should actually be.

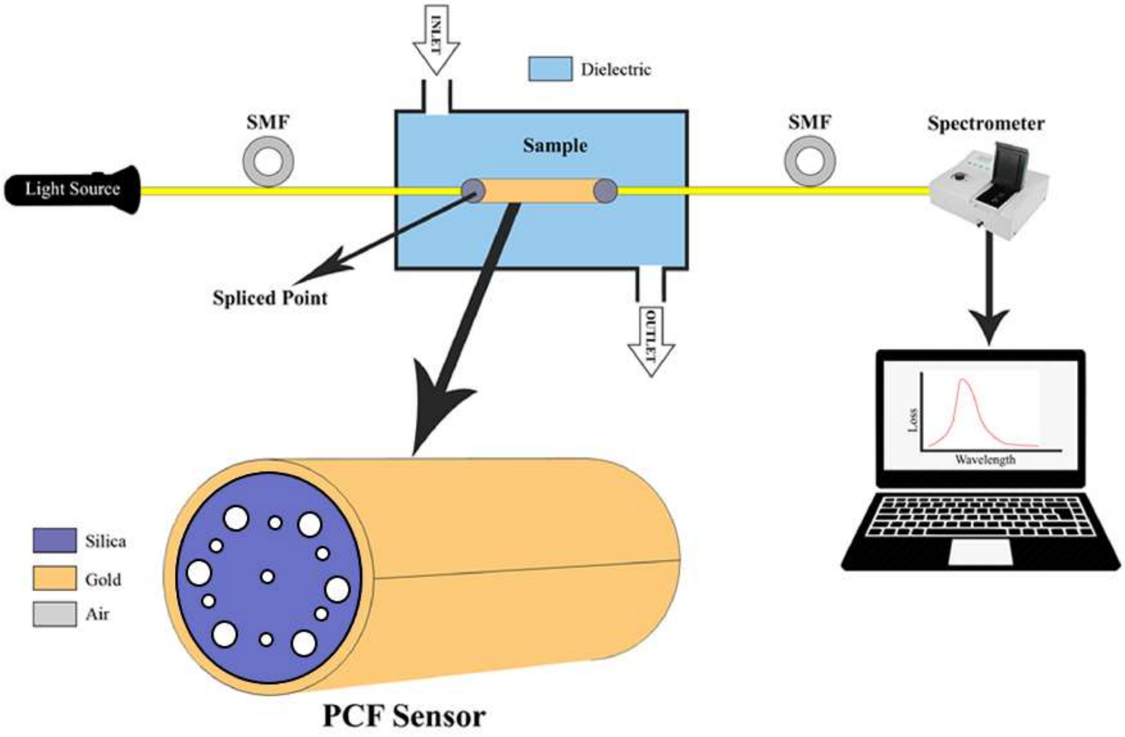

Figure 5.4: Visual illustration of working mechanism of PCF sensor

From the figure above you can see that, analyte is inserted into the analyte layer through the inlet and goes out of the layer using the outlet. That is how the thickness of the layer can be varied by varying the amount of analyte inside the layer. We optimized the analyte layer to get the best possible sensitivity from our sensor hence the analyte layer we got was not thick enough. That is why we needed to optimize the PML layer and we made sure that the thickness of this layer is such that it doesn't influence guiding properties and in turn increase or decrease the sensitivity.

All geometrical parameters have a considerable amount of influence on the sensing performance which is altered by modifying parameters like PML thickness, sensing layer, gold (Au) layer, and pitch. We obtained maximum AS and WS of 1072.5 RIU^{-1} and 41,000 nm/RIU at analyte RI of 1.38 and 1.40 respectively. Birefringence is another critical parameter of a SPR sensor. It signifies the coupling order of a fiber. We obtained birefringence of 0.001. The proposed SPR biosensor projects a simple core design which assists in easy fabrication. The comparative result with prior designs is shown in Table 5.1.

TABLE 5.1

COMPARING RESULTS OF PROPOSED STRUCTURE WITH PRIOR SENSORS

Ref	Sensing Range	AS (RIU^{-1})	Resolution (AS) (RIU)	WS (nm/RIU)	Resolution (WS) (RIU)
[102]	1.33-1.37	266	3.75×10^{-5}	2200	4.5×10^{-5}
[83]	1.33-1.35	72.47	3.97×10^{-5}	2520	3.9×10^{-5}
[82]	1.33-1.38	1411	7.09×10^{-6}	25000	4.00×10^{-6}
[75]	1.33-1.39	1506	6.64×10^{-6}	30000	3.33×10^{-6}
Proposed work	1.33-1.40	1072.5	9.32×10^{-6}	41000	2.4×10^{-6}

5.4 Discussion

A novel hexagonal lattice plasmonic PCF biosensor with external detecting ability has been proposed in this paper. Using the chemical vapor deposition (CVD) method, a plasmonic gold layer can be applied and it will be able to reduce fabrication complexity. The proposed design gives maximal AS of 1072.5 RIU^{-1}, peak WS of 41,000 nm/RIU, and sensor resolution of 2.4×10^{-6} in x-polarization mode. This proposed biosensor can be carried out in numerous biochemical applications due to the upgraded modal properties with a simple yet unique structure.

Chapter 6: Concluding Remarks and Future Studies

6.1 Conclusion

A simple single-layer square lattice plasmonic PCF biosensor is proposed here with external sensing operability. The objective of this research is to put forward a draft based wholly on annular air holes. We have considered all structural parameters to attain the maximum sensitivity and sensor resolution possible. As a general remark, in practical implementations of amplitude sensing mechanism is avoided as it is influenced by the power fluctuations of the source and the detector, as well as optics included. In the case of WS, many cross-sensitivity issues are eliminated. In the next design we tried to reduce the loss and increase sensitivity. The proposed structure forms a single layer of hexagonal-shaped lattice configuration and a layer of plasmonic material. We aimed to get fewer propagation losses undertaking the core guided mode and plasma mode which was obtained by positioning extra small air holes in between the central air holes. One of the main reasons for the novelty of our structure is that it is formed using circular air holes only resulting in comparatively easier fabrication than other structures. Though both of our designs are modeling works, they are fabrication friendly and also they have the potential to be implemented practically.

6.2 Socio-Economic Influence:

Surface plasmon resonance (SPR) is prevalent for around 20 years, even now several researchers still reckon using dated approaches in order to pervade biological interactivity considering the value and complications regarding SPR analysis. With the advancement in SPR-based research, SPR based technology is becoming more economical and attainable which is letting researchers appreciate the practicality of SPR data. It is assumed that SPR will end up becoming a caliber technique obtainable in each and every biochemistry lab since it exhibits the accurate essence of unalterable entanglement. Surface plasmon resonance accords the date to acknowledge the binding interactions amidst biomolecules. One of the principal features of the SPR based technology is the propensity to evaluate the reciprocity between analytes and ligands in the absence of excess time and money on high-priced labeling reagents and protocols. It needs a nominal mass of specimens for experiments on binding kinetics. The sensor chips used in the experiments are reusable which lowers the overall cost. Replication of experiments provides confidence to the researchers in the result accuracy. Detection of plasma, blood, blood components from unspecified specimens is a huge impact on the medical research where SPR sensors are being widely used. Over the last few years, SPR sensing exhibits massive progress through monitoring of drugs, proteins, enzymes, peptides. One of the biggest contributions of SPR sensing in the medical field is the impact it on medical conditions such as Alzheimer’s, diabetes, hepatitis leukemia, breast cancer and prostate cancer etc. by detecting or analyzing the nucleic acids in biofluids retrieved from patients affected by the aforementioned diseases. Food safety has seen a huge advantage due to the advancement of SPR based sensors. They are used to detect the amount of alcohol present in different alcoholic beverages, the concentration of E. coli in addition to polar compounds content in oils. Other than that, pesticide, TNT, aromatic hydrocarbons, phenols, dioxins and residues, pathogens, microbial load, urea, phenolic components, toxic proteins, and heavy metals are detected in food samples.

6.3 Future Studies

Although many PCF sensors are already modeled, not all the challenges for such PCFs are solved like accurate light guiding problem, metal coating problem inside airholes for internal sensing. That is why researchers are still proposing sensors to overcome these challenges. More recently titanium nitride (TiN) based SPR sensors have gained huge popularity because of the plasmonic material’s high melting point and high chemical stability. We can work with other plasmonic materials like TiN, AZO, TiO_2 to further improving the findings in this study. Different types of air holes that could provide better results will be tested in the future. We will also investigate the change in the sensing property by using a bi-metallic layer.

6.4 References

[1] S. Atakaramians, S. Afshar V., T. M. Monro, and D. Abbott. Advances in Optics and Photonics **5**, 169–215 (2013) https://doi.org/10.1364/AOP.5.000169

[2] B. Bowden, J. A. Harrington, and O. Mitrofanov. Opt. Lett. **32**, 2945-2947(2007) . https://doi.org/10.1364/OL.32.002945

[3] A. Dupuis, K. Stoeffler, B. Ung, C. Dubois, and M. Skorobogatiy. J. Opt. Soc. Am. B **28**, 896-907 (2011). https://doi.org/10.1364/JOSAB.28.000896

[4] M. Nagel, A. Marchewka, and H. Kurz. Opt. Express **14**, 9944-9954 (2006). https://doi.org/10.1364/OE.14.009944

[5] Homola, J., Surface Resonance Sensors for Detection of Chemical and Biological Species. Chem. Rev., 108(2): p. 462-493, 2008.

[6] Homola, J., Present and future of surface plasmon resonance biosensors. Analytical and Bioanalytical Chemistry, 377(3): p. 528-539, 2003.

[7] Leidberg, B., et al., Surface Plasmon Resonance for Gas-Detection and Biosensing. Sensors and Actuators, 4(2): p. 299-304, 1983.

[8] Homola, J., et al., Spectral surface plasmon biosensor for detection of staphylococcal enterotoxin B in milk. International Journal of Food Microbiology, 75(1-2): p.61-69, 2002.

[9] Kretschmann, E. and Reather, H. Radiative decay of nonradiative surface plasmon excited by light. Z.Naturf. 23A: 2135-2136; 1968.

[10] Kretschmann, E. Die Bestimmung optischer Konstanten von Metallen durch Anregung von Oberflachenplasmaschwingugnen. Z Phys 241: 313-324; 1971.

[11] Otto, A. Exitation of nonradiative surface plasma waves in silver by the method of frustrated total reflection. Z Phys 216: 398-410; 1968.

[12] Pockrand, I. et al Surface plasmon spectroscopy of organic monolayer assemblies. Surface Sci. 74: 237-244; 1978.

[13] Peterlinz, K. A. and Georgiadis, R. Two-color approach for determination of thickness and dielectric constant of thin films using surface plasmon resonance. Opt.Commun. 130: 260- 266; 1996

[14] Liedberg, B. et al Principles of biosensing with an extended coupling matrix and surface plasmon resonance. Sensors and Actuators B 11: 63-72; 1993.

[15] Zhang, L. and Uttamchandani, D. Optical chemical sensing employing surface plasmon resonance. Electron Lett. 23: 1469-1470; 1988.

[16] Striebel, Ch. et al Characterization of biomembranes by spectral elipsometry, surface plasmon resonance and interferometry with regard to biosensor application. Biosens.Bioelectron. 9: 139-146; 1994.

[17] Lofas, S. and Johnsson, B. A novel hydrogel matrix on gold surfaces in surface plasmon resonance sonsors for fast en efficient covalent immobilization of ligands. J.chem.soc., chem commun. 1526-1528; 1990.

[18] Lofas, S. Dextran modified self-assembled monolayer surfaces for use in biointeraction analysis with surface plasmon resonance. Pure & Appl.Chem. 67: 829-834; 1995.

[19] S. Sjolander and C. Urbaniczky, “Integrated fluid handling system for bio-molecular interaction analysis.” Analytical Chemistry vol. 63, pp. 2338-2345,1991.

[20] Lofas, S. Dextran modified self-assembled monolayer surfaces for use in biointeraction analysis with surface plasmon resonance. Pure & Appl.Chem. 67: 829-834; 1995.

[21] S. Lofas et al “Bioanalysis with surface plasmon resonance.” Sensors and Actuators B vol. 5, pp. 79-84,1991.

[22] R. Karlsson et al “Kinetic analysis of monoclonal antibody-antigen interactions with a new biosensor based analytical system.” Journal of Immunological Methods 229-240; 1991.

[23] K.M. Mc Peak, S.V. Jayanti, S.J. Kress, S. Meyer, S. Iotti, and A. Rossinelli, “Plasmonic films can easily be better: Rules and recipes.” ACS Photonics, vol. 2, pp. 326–333, 2015.

[24] Y. Lu, C.J. Hao, B.Q. Wu, M. Musideke, L.C. Duan, W.Q. Wen, and J.Q. Yao, “Surface plasmon resonance sensor based on polymer photonic crystal fibers with metal nano layers.” Sensors, vol. 13, pp. 956–965, 2013.

[25] B. D. Gupta and R. K. Verma, Surface Plasmon Resonance-Based Fiber Optic Sensors: Principle, Probe Designs, and Some Applications, Journal of Sensors, 2009,1-12,2009.

[26] Zamarreño, C. R., Rivero, P. J., Hernaez, M., Goicoechea, J., Matías, I. R., & Arregui, F. J. Optical Sensors for Corrosion Monitoring. Intelligent Coatings for Corrosion Control, 603–640 ; 2015.

[27] Descrovi, E., Paeder, V., Vaccaro, L., & Herzig, H.-P. A virtual optical probe based on localized Surface Plasmon Polaritons. Optics Express, 13(18), 7017. doi:10.1364/opex.13.007017, 2005.

[28] Ligler, F. S. and Taitt, C. R. (eds), Optical biosensors: today and tomorrow, Elsevier Science, 2008

[29] Raether, H., [Surface plasmons on smooth and rough surfaces and on gratings], Springer, New York, 1988.

[30] Barnes, W. L., Murray, W. A., Dintinger, J., Devaux, E. and Ebbesen, T. W., "Surface plasmon polaritions and their role in the enhanced transmission of light through periodic arrays of subwavelength holes in a metal film," Physical Review Letters 92(10), 107401 ,2004.

[31] Sharma, A. K, Jha, R. and Gupta, B. D., "Fiber-optic sensors based on surface plasmon resonance: a comprehensive review," IEEE Sensors 7(8), 1118-1129 ,2007.

[32] Fan, X., White, I. M., Shopova, S. I., Zhu, H., Suter, J. D. and Sun, Y., "Sensitive optical biosensors for unlabeled targets: a review," Analytica Chimica Acta 620(1-2), 8-26 ,2008.

[33] Wolfbeis, O. S., "Fiber-optic chemical sensors and biosensors," Analytical Chemistry 80(12), 4269-4283 ,2008.

[34] Lee, B., Roh, S. and Park, J., "Current status of micro- and nano-structured optical fiber sensors," Optical Fiber Technology 15(3), 209-221 ,2009.

[35] M. A. Mollah, A. K. Paul and S. M. A. Razzak "Surface Plasmon Resonance based DualPolarized Photonic Crystal Fiber Refractive Index Sensor," 2018 Int. Conf. Adv. Electr. Electron. Eng., pp. 1–4, 2018, Gazipur, Bangladesh.

[36] A. A. Rifat, G. A. Mahdiraji, Y. M. Sua, Y. G. Shee, R. Ahmed, D. M. Chow, & F. R. M. Adrikan," Surface Plasmon Resonance Photonic Crystal Fiber Biosensor: A Practical Sensing Approach," IEEE Photonics Technology Letters, vol.27, no. 15, pp. 1628–1631, 2015.

[37] A. A. Rifat, G. A. Mahdiraji, Y. G. Shee, J. Shawon, and F. R. Mahamd, " A Novel Photonic Crystal Fiber Biosensor Using Surface Plasmon Resonance," Procedia Engineering, vol. 140, pp. 1–7, 2016.

[38] R. K. Gangwar and V. K. Singh, "Highly Sensitive Surface Plasmon Resonance Based DShaped Photonic Crystal Fiber Refractive Index Sensor," Plasmonics, vol. 12, no. 5, pp. 1–6, 2016.

[39] E. Haque, A. Hossain, F. Ahmed, and Y. Namihira, "Surface Plasmon Resonance Sensor Based on Modified D -Shaped Photonic Crystal Fiber for Wider Range of Refractive Index Detection," IEEE Sensors Journal, vol. 18, no.20, pp. 8287 - 8293, 2018.

[40] G. Wang, S. Li, G. An, X. Wang, Y. Zhao, and W. Zhang, "Highly sensitive D-shaped photonic crystal fiber biological sensors based on surface plasmon resonance," Optical Quantum Electronics., vol. 48, no. 1, pp. 1–9, 2016

[41] S. Sharmin, A. Bosu and S. Akhtar, "A Simple Gold-Coated Photonic Crystal Fiber Based Plasmonic Biosensor," 2018 International Conference on Advances in Electronics Engineering, pp. 1–4, 2018, Gazipur, Bangladesh

[42] M. A. Mollah, A. K. Paul, and S. M. A. Razzak, “Dual Polarized Plasmonic Refractive Index Sensor based on Photonic Crystal Fiber,” 2018 10th International Conference on Computer and Electrical Engineering, pp. 73–76, 2018.

[43] S. Islam, J. Sultana, A. Dinovitser, Brian W.-H. Ng, and D. Abbott, “A gold coated plasmonic sensor for biomedical and biochemical analyte detection,” 43rd International Conference on Infrared, Millimeter, and Terahertz Waves (IRMMW-THz), pp. 9–10, Nagoya Congress Center, Japan, 2018.

[44] A. K. Paul, A. Bakar, S. Rahman, S. M. A. Razzak, and A. K. Sarkar, “Hybrid Cladding Structured Gold Coated Photonic Crystal Fiber Biosensor Based on Surface Plasmon Resonance,” 2nd International Conference on Electrical & Electronic Engineering (ICEEE), pp. 1–4, Rajshahi, Bangladesh, December, 2017.

[45] S. Chu et al., “Design and Analysis of Surface Plasmon Resonance based Photonic QuasiCrystal Fibre Biosensor for High Refractive Index Liquid Analytes,” EEE Journal of Selected Topics in Quantum Electronics, vol. 25, no. 2 , pp. 1–8, 2018.

[46] R. Hasan et al., “Spiral Photonic Crystal Fiber-Based Dual-Polarized,” IEEE Sensors Journal, vol. 18, no. 1, pp. 133–140, 2018.

[47] A. Ullah, M. M. S. Hossain, and M. S. Alam, “SPR Biosensor Based on Microstructured Fiber with Lens Shaped Air Holes,” 2017 IEEE International Conference on Telecommunications and Photonics (ICTP), pp. 26–28, 2017, Dhaka, Bangladesh.

[48] M. S. Islam, M. R. Islam, J. Sultana, A. Dinovitser, Brian W.-H. Ng, and D. Abbott, “Exposed Core Localized Surface Plasmon Resonance Biosensor,” Journal of the Optical Society of America B, 36(8), (2019).

[49] Md. M. Rahman, F. A. Mou, M. I. H. Bhuiyan and M. R. Islam, “Photonic crystal fiber based terahertz sensor for cholesterol detection in human blood and liquid foodstuffs,” Sensing and Bio-Sensing Research, (2020).

[50] F. A. Mou, Md. M. Rahman, M. R. Islam and M. I. H. Bhuiyan, “Development of a photonic crystal fiber for THz wave guidance and environmental pollutants detection,” Sensing and Bio-Sensing Research, Volume 29, (2020).

[51] Mohammad Rakibul Islam, Md. Faiyaz Kabir, Khandoker Md. Abu Talha and Md. Saiful Islam, “A novel hollow core terahertz refractometric sensor,” Sensing and Bio-Sensing Research, Volume 25, (2019).

[52] M. S. Islam, J. Sultana, K. Ahmed, M. R. Islam, A. Dinovitser, Brian W.-H. Ng, D. Abbott, “Terahertz detection of alcohol using a photonic crystal fiber sensor,” Applied Optics, vol. 57, no. 10, pp. 2426-33, (2018).

[53] M. S. Islam, J. Sultana, A. Dinovitser, K. Ahmed, M. R. Islam, M. Faisal, W.-H. Ng, D. Abbott, “A Novel Zeonex based photonic sensor for alcohol detection in beverages,” IEEE Inter. Conf. on Telecommunications and Photonics (ICTP), pp. 114-18, (2017).

[54] S. W. James and R. P. Tatam, "Optical fibre long-period grating sensors: characteristics and application," Measurement science and technology 14, R49 (2003).

[55] Dora Juan Juan Hu and Ho Pui Ho, "Recent advances in plasmonic photonic crystal fibers: design, fabrication and applications," Adv. Opt. Photon. **9**, 257-314 (2017)

[56] W. Knoll, “Interfaces and thin films as seen by bound electromagnetic waves,” Annual Review of Physical Chemistry, 49(1), 569-638 (1998)

[57] W. J. Bender and R. E. Dessy, "Surface plasmon resonance sensor," Google Patents (1994).

[58] R. Ahmmed, R. Ahmed and S. M. A. Razzak, "Design of large negative dispersion and modal analysis for hexagonal, square, FCC and BCC photonic crystal fibers," 2013 International Conference on Informatics, Electronics and Vision (ICIEV), Dhaka, pp. 1-6 (2013).

[59] R. A. Aoni, R. Ahmed, and S. M. Abdur Razzak, "Design and Simulation of Duel-Concentric-Core Photonic Crystal Fiber for Dispersion Compensation," *in* 2013 CIOMP-OSA Summer Session on Optical Engineering, Design and Manufacturing,

[60] J. Rolland, J. Wyant, P. Chavel, X. Zhang, C. Wang, and Y. Bai, eds., (Optical Society of America, 2013), paper Tu2.

[61] C. Caucheteur, T. Guo, and J. Albert, "Review of plasmonic fiber optic biochemical sensors: improving the limit of detection," Analytical and bioanalytical chemistry 407, 3883-3897 (2015).

[62] Naik G. V., Shalaev V. M., Boltasseva A., "Alternative plasmonic materials: beyond gold and silver," Adv Mater.;25(24):3264-3294 (2013).

[63] A. A. Rifat *et al*., "Copper-Graphene-Based Photonic Crystal Fiber Plasmonic Biosensor," in IEEE Photonics Journal*,* vol. 8, no. 1, pp. 1-8, Art no. 4800408 (2016).

[64] A. A. Rifat *et al*., "Surface Plasmon Resonance Photonic Crystal Fiber Biosensor: A Practical Sensing Approach," in IEEE Photonics Technology Letters*,* vol. 27, no. 15, pp. 1628-1631, 1 Aug.1, (2015).

[65] Veerpal Kaur, Surindar singh, "Design of titanium nitride coated PCF-SPR sensor for liquid sensing applications", Optical Fiber Technology, Volume 48, Pages 159-164, ISSN 1068-5200, (2019).

[66] Esfahani Monfared. Y, "Refractive Index Sensor Based on Surface Plasmon Resonance Excitation in a D-Shaped Photonic Crystal Fiber Coated by Titanium Nitride," Plasmonics **15,** 535–542 (2020).

[67] Y. Lu, M. T. Wang, C. J. Hao, Z. Q. Zhao and J. Q. Yao, "Temperature Sensing Using Photonic Crystal Fiber Filled With Silver Nanowires and Liquid," in *IEEE Photonics Journal*, vol. 6, no. 3, pp. 1-7, Art no. 6801307 (2014).

[68] Yang, X., Lu, Y., Liu, B. et al., "Analysis of Graphene-Based Photonic Crystal Fiber Sensor Using Birefringence and Surface Plasmon Resonance," Plasmonics **12,** 489–496 (2017).

[69] Nannan Luan, Ran Wang, Wenhua Lv, and Jianquan Yao, "Surface plasmon resonance sensor based on D-shaped microstructured optical fiber with hollow core," Opt. Express **23**, 8576-8582 (2015)

[70] Min Liu, Xu Yang, Ping Shum, and Hongtao Yuan, "High-sensitivity birefringent and single-layer coating photonic crystal fiber biosensor based on surface plasmon resonance," Appl. Opt. **57**, 1883-1886 (2018).

[71] C. Liu *et al.*, "Birefringent PCF-Based SPR Sensor for a Broad Range of Low Refractive Index Detection," in IEEE Photonics Technology Letters, vol. 30, no. 16, pp. 1471-1474, 15 Aug.15, (2018).

[72] Mohammad Al Mahfuz, Md. Rabiul Hasan, Moriom Rojy Momota, Al Masud, and Sanjida Akter, "Asymmetrical photonic crystal fiber based plasmonic sensor using the lower birefringence peak method," OSA Continuum **2**, 1713-1725 (2019).

[73] Guowen An, Xiaopeng Hao, Shuguang Li, Xin Yan, and Xuenan Zhang, "D-shaped photonic crystal fiber refractive index sensor based on surface plasmon resonance," Appl. Opt. **56**, 6988-6992 (2017).

[74] Y. E. Monfared, M. Hajati, C. Liang, S. Yang and M. Qasymeh, "Quasi-D-Shaped Fiber Optic Plasmonic Biosensor for High-Index Analyte Detection," in *IEEE Sensors Journal*, vol. 21, no. 1, pp. 17-23, (2021)

[75] M. A. Mahfuz, M. A. Mollah, M. R. Momota, A. K. Paul, A. Masud, S. Akter, M. R. Hasan, “Highly sensitive photonic crystal fiber plasmonic biosensor: Design and analysis,” Optical Materials, Volume 90, Pages 315-321(2019).

[76] F. Haider, R. A. Aoni, R. Ahmed, M. S. Islam and A. E. Miroshnichenko, "Propagation Controlled Photonic Crystal Fiber-Based Plasmonic Sensor via Scaled-Down Approach," in IEEE Sensors Journal*,* vol. 19, no. 3, pp. 962-969, 1 Feb.1, (2019).

[77] A.A. Rifat, G. Amouzad Mahdiraji, Y.G. Shee, Md. Jubayer Shawon, F.R. Mahamd Adikan, “A Novel Photonic Crystal Fiber Biosensor Using Surface Plasmon Resonance,” Procedia Engineering, Volume 140, Pages 1-7 (2016).

[78] J. N. Dash and R. Jha, "Graphene-Based Birefringent Photonic Crystal Fiber Sensor Using Surface Plasmon Resonance," *in* IEEE Photonics Technology Letters, vol. 26, no. 11, pp. 1092-1095, June1, (2014).

[79] M. S. Islam *et al*., "A Hi-Bi Ultra-Sensitive Surface Plasmon Resonance Fiber Sensor," in *IEEE Access*, vol. 7, pp. 79085-79094, (2019).

[80] Firoz Haider, Rifat Ahmmed Aoni, Rajib Ahmed, and Andrey E. Miroshnichenko, "Highly amplitude-sensitive photonic-crystal-fiber-based plasmonic sensor," J. Opt. Soc. Am. B **35**, 2816-2821 (2018).

[81] Md. Saiful Islam, Jakeya Sultana, Ahmmed. A. Rifat, Rajib Ahmed, Alex Dinovitser, Brian W.-H. Ng, Heike Ebendorff-Heidepriem, and Derek Abbott, "Dual-polarized highly sensitive plasmonic sensor in the visible to near-IR spectrum," Opt. Express **26**, 30347-30361 (2018).

[82] Anna Wang, Andrew Docherty, Boris T. Kuhlmey, Felicity M. Cox, and Maryanne C. J. Large, "Side-hole fiber sensor based on surface plasmon resonance," Opt. Lett. **34**, 3890-3892 (2009)

[83] E. Klantsataya, A. François, H. Ebendorff-Heidepriem, P. Hoffmann, and T. Monro, “Surface Plasmon Scattering in Exposed Core Optical Fiber for Enhanced Resolution Refractive Index Sensing,” *Sensors*, vol. 15, no. 10, pp. 25090–25102, (2015)

[84] W. C. Wong *et al*., "Photonic Crystal Fiber Surface Plasmon Resonance Biosensor Based on Protein G Immobilization," in *IEEE Journal of Selected Topics in Quantum Electronics*, vol. 19, no. 3, pp. 4602107-4602107, (2013)

[85] Mohammad Rakibul Islam, A. N. M. Iftekher, Kazi Rakibul Hasan, Md. Julkar Nayen, and Saimon Bin Islam, "Dual-polarized highly sensitive surface-plasmon-resonance-based chemical and biomolecular sensor," Appl. Opt. **59**, 3296-3305 (2020).

[86] A. Vial, A.-S. Grimault, D. Macías, D. Barchiesi, and M. L. de La Chapelle, "Improved analytical fit of gold dispersion: Application to the modeling of extinction spectra with a finite-difference time-domain method," Physical Review B **71**, 085416 (2005).

[87] J. A. Sazio, A. Amezcua-Correa, C. E. Finlayson, J. R. Hayes, T. J. Scheidemantel, N. F. Baril, B. R. Jackson, Dong-Jin Won, F. Zhang, E. R. Margine, V. Gopalan, V. H. Crespi, J. V. Badding, “Microstructured Optical Fibers as High-Pressure Microfluidic Reactors,” *Science,* Vol. 311, Issue 5767, pp. 1583-1586 (2006).

[88] E. K. Akowuah, T. Gorman, H. Ademgil, S. Haxha, G. K. Robinson and J. V. Oliver, "Numerical Analysis of a Photonic Crystal Fiber for Biosensing Applications," in *IEEE Journal of Quantum Electronics*, vol. 48, no. 11, pp. 1403-1410, Nov. (2012).

[89] Z. Li, Z. Yu, Y. Shen, X. Ruan and Y. Dai, "Graphene Enhanced Leaky Mode Resonance in Tilted Fiber Bragg Grating: A New Opportunity for Highly Sensitive Fiber Optic Sensor," in *IEEE Access*, vol. 7, pp. 26641-26651, (2019).

[90] A. Nooke, U. Beck, A. Hertwig, A. Krause, H. Krüger, V. Lohse, D. Negendank, J. Steinbach, “On the application of gold based SPR sensors for the detection of hazardous gases,” Sensors and Actuators B: Chemical, Volume 149, Issue 1, Pages 194-198, (2010).

[91] R. Otupiri, E. K. Akowuah, S. Haxha, H. Ademgil, F. AbdelMalek and A. Aggoun, "A Novel Birefrigent Photonic Crystal Fiber Surface Plasmon Resonance Biosensor," in *IEEE Photonics Journal*, vol. 6, no. 4, pp. 1-11, Aug. (2014).

[92] Mahfuz, M.A.; Hossain, M.A.; Haque, E.; Hai, N.H.; Namihira, Y.; Ahmed, F. A Bimetallic-Coated, Low Propagation Loss, Photonic Crystal Fiber Based Plasmonic Refractive Index Sensor. *Sensors 19*, 3794 (2019).

[93] Meng, Q.-Q.; Zhao, X.; Lin, C.-Y.; Chen, S.-J.; Ding, Y.-C.; Chen, Z.-Y. Figure of Merit Enhancement of a Surface Plasmon Resonance Sensor Using a Low-Refractive-Index Porous Silica Film. *Sensors 17*, 1846 (2017).

[94] M. S. Islam, J. Sultana, K. Ahmed, A. Dinovitser, M. R. Islam, B. W.-H. Ng and D. Abbott “A novel approach for spectroscopic chemical identification using photonic crystal fiber in the terahertz regime,” IEEE Sensors Journal **18**(2), 575–582, (2018)

[95] Md. Aminul Islam, M. Rakibul Islam, Md. Moinul Islam Khan, J. A. Chowdhury, F. Mehjabin, and Mohibul Islam, “Highly Birefringent Slotted Core Photonic Crystal Fiber for THz Wave Propagation,” Phys. Wave Phen., vol. 28, no. 1, pp. 58–67, (2020).

[96] Md. Rabiul Hasan, Sanjida Akter, Ahmmed A. Rifat, Sohel Rana, Kawsar Ahmed, Rajib Ahmed, Harish Subbaraman, Derek Abbott, “Spiral Photonic Crystal Fiber-Based Dual-Polarized Surface Plasmon Resonance Biosensor”, IEEE Sensors Journal, vol. 18, no. 1, January 1, (2018).

[97] C. Liu, W. Su, Q. Liu, et al., “Symmetrical Dual D-Shape Photonic Crystal Fibers for Surface Plasmon Resonance Sensing,” Optics Express 26(7) 9039–9049 (2018).

[98] Xin Chen, Li Xia, Li Chen, “Surface Plasmon Resonance Sensor Based on A Novel D Shaped Photonic Crystal Fiber for Low Refractive Index Detection,” IEEE Photon. J. 10 (1) (2018).

[99] G. A. Mahdiraji, D. M. Chow, S. R. Sandoghchi, F. Amirkhan, E. Dermosesian, K. S. Yeo, Z. Kakaei, M. Ghomeishi, S. Y. Poh, S. Y. Gang, F. R. M. Adikan, “Challenges and Solutions in Fabrication of Silica-Based Photonic Crystal Fibers: An Experimental Study,” Fiber and Integrated Optics, 33:1-2, 85-104 (2014).

[100] X. Yu, Y. Zhang, S. Pan, P. Shum, M. Yan, Y. Leviatan, and C. Li, "A selectively coated photonic crystal fiber-based surface plasmon resonance sensor," Journal of Optics 12, 015005 (2009).

[101] Rifat A.A., Rabiul Hasan M., Ahmed R., Miroshnichenko A.E., “Microstructured Optical Fiber-Based Plasmonic Sensors,” In: Hameed M., Obayya S. (eds) Computational Photonic Sensors. Springer, Cham. (2019).

[102] D. Pysz, I. Kujawa, R. Stepien, M. Klimczak, A. Filipkowiski, M. Franczyk, L. Kociszewski, J. Buzniak, K. Harasny, and R. Buczynski, “Stack and draw fabrication of soft glass microstructured fiber optics”, Bulletin of the Polish Academy of Sciences: Technical Sciences, Vol. 62, No. 4, (2014).

[103] A. A. Rifat, R. Ahmed, G. A. Mahdiraji, F. M. Adikan, and A. E. Miroshnichenko, "Highly sensitive selectively coated photonic crystal fiber-based plasmonic sensor," Optics letters 43, 891-894 (2018).

[104] J. Xue, S. Li, Y. Xiao, W. Qin, X. Xin, and X. Zhu, “Polarization filter characters of the gold-coated and the liquid filled photonic crystal fiber based on surface plasmon resonance” Opt. Exp. 21(11), 13733–13740, (2013).

[105] S. Patskovsky, M. Meunier, P. N. Prasad, and A. V. Kabashin, "Self-noise-filtering phase-sensitive surface plasmon resonance biosensing," Optics Express 18, pp. 14353-14358,2010.

[106] X. D. Hoa, A. G. Kirk, and M. Tabrizian, "Towards integrated and sensitive surface plasmon resonance biosensors: A review of recent progress," Biosensors & Bioelectronics 23, pp 151-160,2007

[107] F. Zolla, G. Renversez, A. Nicolet, B. Kuhlmey, S. Guenneau, and D. Felbacq, Fundamentals of Photonic Crystal Fibers. London, U.K.: Imperial College Press, 2005

[108] Chiavaioli, F., Gouveia, C.A.J., Jorge, P.A.S., Baldini, F., “Towards a Uniform Metrological Assessment of Grating-Based Optical Fiber Sensors: From Refractometers to Biosensors,” Biosensors, 7, 23, 2017.